Influence of Anthropogenic Nutrient Inputs on Rates of Coastal Ocean Nitrogen and Carbon Cycling in the Southern California Bight, USA

Karen McLaughlin[1*], Meredith D.A. Howard[1,2], George Robertson[3], Carly D.A. Beck[1,4], Minna Ho[1], Fayçal Kessouri[1], Nikolay P. Nezlin[1,5], Martha Sutula[1], Stephen B. Weisberg[1]

*Corresponding author

[1]Southern California Coastal Water Research Project

[2]now at: California Region 5, Central Valley Regional Water Quality Control Board

[3]Orange County Sanitation District

[4]now at: California Department of Fish and Wildlife

[5]now at: RBR, Ltd.

For submission to Elementa

https://www.elementascience.org/

Abstract

Coastal nitrogen (N) enrichment is a global environmental problem that can influence acidification, deoxygenation, and subsequent habitat loss in ways that can be synergistic with global climate change impacts. In the Southern California Bight, an eastern boundary upwelling system, modeling of wastewater discharged through ocean outfalls has shown that it effectively doubles N loading to urban coastal waters. However, effects of wastewater outfalls on biogeochemical rates of primary production and respiration, key processes through which coastal acidification and deoxygenation are manifested, have not been directly linked to observed trends in ambient chlorophyll *a,* oxygen and pH. In this paper, we compare observations of nutrient concentrations and forms, as well as rates of biogeochemical cycling, in areas within treated wastewater effluent plumes compared to areas spatially distant from ocean outfalls where we expected minimum influence of the plume. We document that wastewater nutrient inputs have an immediate, local effect on nutrient stoichiometry, elevating ammonium and nitrite concentrations by a mean of 4 µM and 0.2 µM, respectively, increasing dissolved nitrogen: phosphorus ratios by a mean of 7 and slightly increasing chlorophyll *a* by a mean of 1 µg L^{-1} in the upper 60 m of the watercolumn*,* as well as increasing rates of nitrification within the plume by a mean of 17 nmol L^{-1} day^{-1} and increasing $\delta^{13}C$ and $\delta^{15}N$ of suspended particulate matter, an integrated measure of primary production, by a mean of 1.3 ‰ and 1 ‰, respectively. We did not observe a significant near plume effect on $\delta^{18}O$ and $\delta^{15}N$ of the dissolved nitrate+nitrite, an indicator of nitrate+nitrite assimilation into the biomass, instantaneous rates of primary production and respiration, or dissolved oxygen concentration, suggesting any potential impact from wastewater on these is moderated by other factors, notably mixing of water masses. These results indicate that a “reference-area” approach, wherein stations within or near the zone of initial dilution (ZID) from the wastewater outfall are compared to stations farther afield (reference areas) to assess contaminant impacts, may be insufficient to document regional scale impacts of nutrients.

Introduction

Globally, offshore ocean outfalls have been considered an effective and reliable strategy for disposing of treated industrial and domestic wastewater (Wood et al. 1993, Roberts et al. 2010). However, wastewater effluent released through these outfalls are rarely treated to remove nutrients and, consequently, they have been implicated in eutrophication of coastal waters (Roberts et al. 2010, Powley et al. 2016, Valiela et al. 2016). Eutrophication can have impacts on coastal habitats that can be synergistic with global changes, such as increasing frequency and occurrence of algal blooms (Howarth et al. 2002, Glibert et al. 2006), coastal acidification (Borges and Gypens 2010, Wallace et al. 2014), and deoxygenation (Rabalais et al. 2014, Breitburg et al. 2018) through enhanced heterotrophic respiration rates. Given appropriate light and temperature conditions, eutrophication initially causes a temporary drawdown of CO_2 concentrations at the surface due to the intense biological productivity of the associated algal bloom (Borges and Gypens 2010). Subsequently, eutrophication lowers pH, because it provides conditions for greater heterotrophic respiration rates (i.e., decomposition, also referred to as remineralization) by organisms such as bacteria. This respiration process oxidizes organic matter, draws down local oxygen levels, releases CO_2, and—in extreme cases—can lead to hypoxic dead zones (Diaz and Rosenberg, 2008). The depth of the pH change associated with anthropogenic eutrophication is a function of where organic matter is respired. In many shallow coastal shelf systems, this acidification occurs at or near the bottom sediments, where organic matter is oxidized (Waldbusser et al. 2010, Sunda and Cai 2012). In the absence of global strategies to mitigate coastal ocean changes, local managers are being urged to consider the management of local, land-based nutrient sources to slow the progression of acidification and deoxygenation and their impact on coastal habitats (Kelly et al. 2011, Strong et al. 2014, Chan et al. 2016).

The role of coastal nutrient discharges and coastal eutrophication in exacerbating coastal acidification and deoxygenation (CAD) is well documented, including the East China Sea and the Gulf of Mexico (Cai et al. 2011), the Baltic Sea (Sunda and Cai 2012), the nearshore regions of the North Sea (Provoost et al. 2010), and the Chesapeake Bay (Waldbusser 2011). However, in an Eastern Boundary Upwelling System (EBUS), strong upwelling and vigorous

surface currents have been thought to limit the impacts of local anthropogenic nutrient inputs (Chavez and Messié 2009, Capone and Hutchins 2013, Fennel and Testa 2019). Recent evidence from the Southern California Bight (SCB) has challenged this thinking along this highly urbanized coastline. In the SCB, on an annual basis, 92% of terrestrial N flux is wastewater effluent from Publicly Owned Treatment Works (POTWs), most of which is discharged directly into coastal waters via a relatively small number of outfall pipes (Sutula et al. 2020). Modeled outfall N loads are roughly equivalent to those from upwelling in urbanized sections of the coast, effectively doubling N loading to the shelf (Howard et al. 2014). These inputs have an immediate, local effect on nitrification rates as high concentrations of wastewater ammonium are rapidly nitrified in the subsurface plumes (McLaughlin et al. 2017). More broadly, observational evidence has shown an increase in the extent of algal blooms in the SCB over the last decade, with chronic blooms documented in areas co-located with major inputs of anthropogenic nutrients (Schnetzer et al. 2007a, Nezlin et al. 2012, Schnetzer et al. 2013). Analysis of a decade of quarterly ocean surveys across the central and northern SCB have shown a significant decrease in dissolved oxygen (DO) concentrations (Bograd et al. 2008), and the rate of decline in the nearshore, proximal to treated wastewater effluent outfalls, has been faster than offshore regions (Booth et al. 2014). However, these regional-scale observations can also be influenced by climate change and Pacific Basin-scale drivers (Booth et al. 2014, Nezlin et al. 2018) and ambient chlorophyll *a*, DO and pH have not been specifically linked to an effect of wastewater outfalls on biogeochemical rates of primary production and respiration – key processes through which CAD are manifested.

In this paper, we quantified nutrient concentrations, forms, and rates of carbon and nitrogen cycling that ultimately influence processes leading to eutrophication and CAD both within wastewater plumes and in areas spatially distant from plumes. We also explored the environmental factors that may be influencing rates, including seasonal and interannual variability linked to the influence of upwelling. Finally, we employed stable isotope tracers to further track relationships and patterns in N and C biogeochemical cycling in these coastal zones as more integrated measurements to compare to the instantaneous rate measurements. We focused on the effect of wastewater N because the SCB is largely N-limited

(Thomas et al. 1974, Cullen and Eppley 1981) and wastewater point source discharges dominate anthropogenic sources (Howard et al. 2014) and contain high concentrations of nitrogenous species. As a core part of our study design, observations of ambient ocean state and rates were made in two types of regions defined by the probability of plume impact: 1) "nearfield" regions, defined as the region of active effluent plume mixing and dispersion within 10 km of the outfall and 2) "farfield" regions, defined as the region where ambient ocean flow and biogeochemical conditions dominate and the effluent plume is expected to exert minimum influence on carbon and nitrogen cycling.

The value of such observations extends beyond testing of the hypothesis of an effect of wastewater plumes on watercolumn biogeochemical parameters (pH, dissolved oxygen, chlorophyll *a*) and rates of nutrient and carbon cycling. To support California's climate action strategies, a spatially-explicit, 3-dimensional numerical ocean model of the SCB was developed and is being applied to examine the relative effects of climate change, natural climate cycles, and local terrestrial and atmospheric carbon and nutrient inputs (Deutsch et al. in review, Kessouri et al. in press). However, in order to support conversations on the utility of nutrient management as a climate change mitigation strategy, such models must be carefully validated against observations of biogeochemical state and rate data. Inadequate numerical model validation has been identified as a significant barrier to effective, evidence-based solutions to coastal eutrophication (Boesch 2019). Models must not only successfully reproduce observed state data, they must also successfully reproduce observed biogeochemical rate data, ensuring that the model is predicting the appropriate state variables for the right reasons. Thus, these observations are part of a coupled observational-numerical modeling approach characterizing the effect of local nutrient and carbon inputs on SCB coastal habitats, laying the foundation for evidence-based solutions for CAD.

Materials and Methods

Study Region

The Southern California Bight (SCB) is the bend in the coastline between Point Conception (~34° 34'N) and the U.S.-Mexico International Border (~32° 32'N). It is situated in

the California Current System on the U.S. Pacific Coast. As an EBUS, the SCB is a biologically productive region of high economic and ecological importance. Seasonal spring upwelling of nutrient-rich deep water maintains high rates of biological productivity over broad scales. At the same time, upwelling draws water masses that are low in DO, pH, and carbonate saturation state (Ω_{Ar}) onto the shelf and into the photic zone (Sutton et al. 2017). Southern California has a Mediterranean climate with surface runoff confined mostly to the winter, rainy season. The SCB is home to one of the most densely populated coastal regions in North America, where the discharges of treated (advanced primary or secondary) wastewater from a population of 20 million people are released to the coastal zone via ocean outfalls, along with the urban and agricultural runoff from 72 rivers (Sutula et al. 2020). Modeling efforts have shown that these nutrient sources rival natural upwelling in magnitude (Howard et al., 2014), roughly doubling available N to nearshore coastal waters on an annual basis.

Study Design

The study was designed to characterize effects of wastewater plumes on state and rate variables in regions nearfield (within-plume) and farfield (spatially distant) from ocean outfalls where treated wastewater effluent is discharged to the highly urbanized, central portion of the SCB (Figure 1). We hypothesized that chemical and biological rates and water chemistry would differ between areas near ocean outfalls (nearfield), where treated wastewater plume was detected, compared to farfield, "reference" areas, where the plume could not be detected. Selection of nearfield and farfield locations was informed by previous studies that used colored dissolved organic matter (CDOM) as a tracer of effluent plume (Rogowski et al. 2013, Nezlin et al. 2020); as a rule of thumb, nearfield stations were generally within 10 km of the outfalls, while farfield stations were greater than 10 km away.

We compared water column nutrient profiles and stable isotopic compositions, rates of nitrification, primary production and respiration in nearfield and farfield regions, as well as relationships between parameters and rates and seasonal and interannual differences thereof. Four sub-regions were sampled, including two nearfield sub-regions near Orange County Sanitation District's (OCSD) and Los Angeles County Sanitation District's (LACSD) ocean outfalls,

a nearshore, farfield sub-region off the coast of northern San Diego County (Camp Pendleton), and an offshore, farfield sub-region off the coast of Los Angeles and Orange Counties (Table 1 and Figure 1). Two stations were sampled in each sub-region for the full suite of measurements and rate analyses. For the nearfield regions, sampling was dynamic and based on currents to enable sampling within the plume. A fixed sampling station was located directly over the outfall pipe and a second site, which varied according to currents, was located a short distance from the outfall, but still within the plume. One additional fixed station was sampled in each effluent-plume sub-region for water column nutrients and stable isotope analysis only (no rate data). For the farfield coastal subregion, one station was located on the continental shelf and the other on the shelf-break. For the offshore farfield subregion, one was located at the San Pedro Ocean Time Series (SPOTS) station (offshore of LACSD's outfall) and the other at the California Cooperative Oceanic Fisheries Investigations (CalCOFI) sample station 90.30 (offshore of OCSD's outfall), both within the San Pedro Basin.

Comparisons and relationships were investigated seasonally, both when wastewater discharge was anticipated to constitute a minor fraction of the total N pool (Spring upwelling period) and a major fraction (late Summer, when the water column is stratified). Four seasons were collected over two years: late Summer stratification in 2014 and 2015, and Spring upwelling in 2015 and 2016. Cruises and rate measurements were conducted over a four-week period in each season; one sub-region sampled per week.

Sample Collection

Vertical profiles were collected at each station using a Sea-Bird Electronics, Inc., SBE911plus (24 Hz) or SBE-25 (8 Hz) conductivity-temperature-depth (CTD) system, measuring a suite of oceanographic properties including pressure, temperature, salinity, colored dissolved organic matter (CDOM), dissolved oxygen, pH, and chlorophyll fluorescence and transmissivity. In addition to the experimental stations, CTD casts were also taken at several stations in the nearfield sub-regions to map the location of the plume and regional hydrodynamics at the time of sampling (Figure SI.1). The profiles were averaged to 1 m bins. Regional climatologies of temperature, salinity, dissolved oxygen, chlorophyll *a*, and CDOM were generated by

interpolation using the Barnes algorithm (Koch et al. 1983) from the R package "oce" (Kelley and Richards 2017).

Discrete samples were collected from Niskin bottles (1.5 and 3 L) on a rosette deployed with the CTD sensor package. Sampling was adaptive at each site, with sample depths determined from downcast CTD observations to identify key oceanographic features at each station (CDOM to mark the plume and chlorophyll *a* maxima). Generally, samples were collected from 5 depths at the stations > 50 m depth: the surface, subsurface chlorophyll maximum layer (depth of highest recorded chlorophyll fluorescence), the center of the thermocline (mixed layer, where the temperature gradient exceeds -0.3 °C m^{-1}), below the thermocline, and at the "bottom" (2-5 m from the sediment surface or the end of the rosette cable, which was either 200 m [OCSD, LACSD] or 300 m [Camp Pendleton]). At shallower stations, four samples were collected from the surface, subsurface chlorophyll maximum, the thermocline, and the bottom. For the nearfield sub-regions, the station over the outfall remained fixed throughout the study, but the "off-outfall/second nearfield" station varied based on currents and was identified using CTD profiles of CDOM from several stations (Figure SI.1). CDOM has been shown to be a reasonable tracer for subsurface effluent plumes (Rogowski et al. 2012, Rogowski et al. 2013, Nezlin et al. 2020).

Field water samples were transferred from the Niskin bottles using acid-washed Tygon tubing into acid-washed 2 L high density polyethylene (HDPE) bottles that were triple rinsed with sample water before filling. Both LACSD and OCSD also supplied samples of effluent for analysis prior to each sampling event in their respective nearfield subregions. These samples were collected as a composite over 24 hours in an acid washed 1 L HDPE bottle. Effluent was stored at 4 °C while the composite was generated.

Sub-samples from both field water and effluent were collected for the suite of dissolved inorganic nutrients (nitrate+nitrite, nitrite, ammonium, and ortho-phosphate), total dissolved nitrogen and phosphorus (TDN, TDP), and dual nitrogen and oxygen isotope ratios for dissolved nitrate+nitrite. In addition, field water was sub-sampled for particulate organic matter concentrations (particulate nitrogen, particulate phosphorus, and particulate organic carbon), stable isotope ratios of carbon and nitrogen of particulate organic matter, and

chlorophyll *a*. Subsamples were frozen immediately. Suspended particulate samples were collected by vacuum filtration onto pre-combusted (450 °C for 4 hours) glass fiber filters (Whatman GF/F). Suspended particulate samples were sub-sampled from the whole water sample and stable isotope analyses and were filtered onboard the cruise and frozen immediately. Filters were collected into snap-close petri dishes and stored in Ziploc bags on ice in the dark for transport. Filters in the petri dishes were dried at 50 °C in the dark until analysis.

Sub-samples for nutrient and nitrate stable isotope analysis were hand-filtered through a 0.45 µm polycarbonate filter (Millipore) and collected in triple-rinsed, 60 mL HDPE amber bottles, stored on ice for transport to the laboratory, and frozen until analysis (Wankel et al. 2006, Wankel et al. 2007, Santoro et al. 2010). Whole water for primary production and nitrification rate incubations were collected directly into acid-washed, triple-rinsed, 2 L HDPE bottles and stored on ice in the dark until the incubations could begin in the laboratory within 6 hours of collection. Whole water for respiration rates was collected into 300 mL borosilicate glass biological oxygen demand bottles that were overfilled with twice the volume of the bottle. Water samples for the rate experiments (primary production, respiration, and nitrification) were stored on ice and in the dark until they were brought back to the lab for experimental preparation.

Laboratory Analyses

Nutrient concentrations. Discrete samples were analyzed for a suite of dissolved nutrients. Nitrate + nitrite, nitrite, soluble reactive phosphate, and ammonium were analyzed using flow injection analyses (FIA, Lachat Instruments, QuikChem 8000 at the Marine Science Institute, at the University of California, Santa Barbara), ammonium was also measured following the protocols of Holmes et al. (1999), total N (TN) and phosphorus (TP) samples were analyzed following persulfate digestion (Patton and Kryskalla 2003) using FIA. A relative assessment of nutrient limitation, N*, was calculated, which represents the deviation in "Redfield" N:P stoichiometry due to additional sources and sinks of nitrate (Deutsch et al. 2001):

$$N^* = [NO_3^-] - (16 * [PO_4^{3-}]) + 2.9 \quad \text{(Eq 1).}$$

Positive N* values reflect regions with a source of nitrate (via nitrogen fixation) and negative N* reflects a sink of nitrate (due to denitrification). Values near zero are consistent with "Redfieldian" assimilation and nitrification of organic matter or that source and loss terms are balanced (Gruber and Sarmiento 1997).

Stable Isotope Analyses. The stable isotopic compositions of dissolved nitrate and nitrite ($\delta^{15}N_{NO2+NO3}$ and $\delta^{18}O_{NO2+NO3}$), ammonium ($\delta^{15}N_{NH4}$), and suspended particulate matter ($\delta\,^{15}N_{PN}$ and $\delta\,^{13}C_{PN}$) are natural tracers of N sources and cycling in the ocean. Variation in the isotopic composition is attributable to distinct source signatures and the mass dependent isotopic discriminations associated with various biogeochemical transformations that constitute the marine N cycle. Because each pathway causes a characteristic shift in isotope composition of the products and reactants, the isotopic composition of the dissolved and particulate pools can provide useful information on the mechanism of these transformations (Sigman et al. 2005, Wankel et al. 2007, Sugimoto et al. 2009).

The preparation and isotope analysis ($\delta^{15}N_{NO2+NO3}$, $\delta^{18}O_{NO2+NO3}$) of dissolved nitrate+nitrite in discrete water samples was performed using a bacterial denitrification assay (Sigman et al. 2001, Casciotti et al. 2002). Samples with at least 0.002 mg/kg as N were analyzed by bacterial conversion of nitrate to nitrous oxide and sub-sequent measurement on a continuous flow isotope ratio mass spectrometer (Sigman et al., 2001; Casciotti et al., 2002; Coplen et al.,2007). Isotope ratios of $^{15}N/^{14}N$ and $^{18}O/^{16}O$ were measured using a ThermoFinnigan GasBench + PreCon trace gas concentration system interfaced to a ThermoScientific Delta V Plus isotope-ratio mass spectrometer at the Stable Isotope Laboratory at the University of California, Riverside. Dissolved ammonium was extracted from 250 mL of wastewater effluent onto glass fiber filter "traps" (Holmes et al. 1998, Hannon and Böhlke 2008) and the isotope ratios of $^{15}N/^{14}N$ were measured using a coupled Costech Elemental Analyzer with a Finnigan Delta Plus Advantage in Continuous Flow Mode at the Stable Isotope Laboratory at the University of California, Riverside. The isotope ratios of $^{15}N/^{14}N$ and $^{13}C/^{12}C$ from suspended particulate matter collected on precombusted Whatman GF/F were measured using a coupled Costech Elemental Analyzer with a Finnigan Delta Plus

Advantage in Continuous Flow Mode at the Stable Isotope Laboratory at the University of California, Riverside. Isotope ratios are reported relative to standards: N_2 in air for $\delta^{15}N$, Vienna Standard Mean Ocean Water (VSMOW) for $\delta^{18}O$, and Vienna Pee Dee Belemnite (VPDB) for $\delta^{13}C$. The standard deviation of replicate standards for particulate material $\delta^{13}C$ was 0.084 ‰ and $\delta^{15}N$ was 0.165 ‰, and the relative percent difference between measured standards and reference values was 0.32% and 0.88%, respectively. The standard deviation of replicate standards for dissolved nitrate $\delta^{18}O$ was 0.17 ‰ and $\delta^{15}N$ was 0.15 ‰, and the relative percent difference between measured standards and reference values was 0.46% and 0.04%, respectively.

Rate Measurements

Primary production rate measurements. Short-term incubations of natural plankton communities were conducted to determine rates of primary production using radioactive ^{14}C labeled compounds, expressed as mg C m^{-3} day^{-1} or integrated vertically to units of mg C m^{-2} day^{-1}. Primary production was assessed at multiple depths bracketing the euphotic zone, collecting four depths from light levels from 95% to 1%: including the surface, the mixed layer, the chlorophyl maximum layer, and the 1% light level. Primary production was estimated from ^{14}C uptake using a simulated *in situ* technique in which the assimilation of dissolved inorganic carbon by phytoplankton yields a measure of the rate of photosynthetic primary production in the euphotic zone (Anderson et al. 2006, Brzezinski and Washburn, 2011). Water was collected from Niskin bottles into 2 L HDPE bottles wrapped in black electrical tape and kept in darkened coolers until transported to the laboratory. Depths included: surface, the chlorophyll maximum, the center of the thermocline, and the 1% light level (three times the Secchi depth). Subsamples from each depth were separated into two acid-cleaned 250 mL polycarbonate bottles; one bottle was wrapped in black electrical tape to measure dark ^{14}C uptake and the other was left open to light but darkened to expected ambient light levels using a neutral density screen. Bottles were incubated for 24 hours after inoculation with ^{14}C sodium bicarbonate in incubators placed outside in ambient light in the Southern California Coastal Water Research Project facility, held at recorded *in situ* seawater temperatures by circulating

incubator water through chillers. At the end of incubations total radioactivity in each sample was determined by adding 250 µL of incubated seawater to 250 µL of β-phenethylamine in a 20 mL glass scintillation vial followed by 10 mL of Ultima Gold XR scintillation cocktail. Each vial was shaken vigorously for 30 s and ^{14}C activity assayed after bubbles had cleared and chemoluminescence had subsided (~2 hours) by a liquid scintillation counter using an internal quench curve. A 50 mL subsample of incubated water was also filtered through a pre-combusted 25 mm Whatman GF/F filter. Filters were placed in individual 20 mL glass scintillation vials and 0.25 mL of 0.5 N HCl was pipetted onto each filter in a fume hood to drive off excess tracer. Vials were left uncapped for a minimum of 7 hours, and 10 mL of Ultima Gold XR scintillation cocktail was added to each vial, the vials capped and shaken, and ^{14}C activity was analyzed by scintillation counting on a scintillation counter using an internal quench curve. Primary productivity rates in both the light and dark incubations were calculated as described by Anderson et al. (2006) and Brzezinski and Washburn (2011). Daily primary production (g C m^{-3} d^{-1}) was calculated as the difference in productivity between light and dark bottles. Productivity-to-biomass ratio was calculated as the daily primary productivity (g C m^{-3} d^{-1}) per unit chlorophyll *a* (g chl a m^{-3}) with units of gC (g chl a)$^{-1}$ d^{-1}. Integrated rates of productivity were calculated using the trapezoidal method.

Respiration rate measurements. Respiration rates were measured at four depths: the chlorophyll maximum, the middle of the thermocline, below the thermocline, and 2 m above the bottom/end of the CTD cable. Whole water was collected from Niskin bottles into 300mL glass bottles, each of which was wrapped in black electrical tape, using acid-cleaned Tygon tubing, overfilling each bottle with at least twice the volume. Three bottles were collected for respiration rate measurements at each depth. An additional 50 mL syringe of whole water was collected from each Niskin bottle and held in a cooler. An initial dissolved oxygen concentration (mg O L^{-1}) and percent oxygen saturation was recorded in the field for each bottle using a YSI ProDO optical dissolved oxygen probe, immediately after bottles were filled. Because the probe displaced some water from each bottle, water was replaced with whole water from the syringe to eliminate headspace in each bottle. Bottles were then stoppered and placed in refrigerated units held at *in situ* water temperatures. Bottles were incubated for

24-48 hours and a final dissolved oxygen concentration (mg L^{-1}) and percent oxygen saturation in each bottle was recorded. Respiration rates were calculated for each depth at in situ temperatures as the difference between time zero oxygen concentrations and final incubated oxygen concentrations.

Nitrification rate measurements: Nitrification is the sequential oxidation of NH_4^+ to NO_3^- via NO_2^-. Nitrification rates were determined by measuring the accumulation of ^{15}N in the dissolved nitrate pool following addition of isotopically-enriched ammonium to bottle incubations (Santoro et al. 2010). Water was collected from Niskin bottles into 2 L HDPE bottles at four depths: the chlorophyll maximum layer, the middle of the thermocline, below the thermocline, and 2 m above the bottom/end of the CTD cable. Subsamples from this initial sample were separated into three 500 mL acid-washed polycarbonate bottles wrapped in black tape. An enriched (99%) tracer of ^{15}N-ammonium chloride was added to a final concentration of 100 nM to two of the bottles and a third bottle without the tracer served as a control. Not knowing ammonium concentrations beforehand, we targeted this concentration to minimize impact on nitrogen cycling within the bottles. The range of percentage labeled ammonium from 0.01 to 1.5%, with a median value of 0.1%. Bottles were incubated in the dark to minimize N uptake by phytoplankton and as close to *in situ* temperature conditions as possible (within ± 2˚C) in a series of refrigerated incubator units. For reference, Q_{10} values for nitrification are on the order of 2-3 (Henriksen 1988). Subsamples of 50 mL each were collected at four-time points (approximately 0, 12, 24, and 36 hours post spike addition), syringe filtered through 0.45 µm filters and frozen until analysis for dissolved nitrate concentration and the isotopic composition of nitrate+nitrite ($\delta^{15}N_{NO2+NO3}$) as described above. Potential nitrification rates were determined by modeling the ^{15}N and ^{14}N contents of the combined nitrate and nitrite pool with inputs from the labeled ammonium pool and outputs through nitrate and nitrite uptake as described in Santoro et al. (2010). Data fitting for the ^{15}N and ^{14}N values measured at each time point was performed by non-linear least squares regression method using MATLAB 8.2 and Statistics Toolbox 8.3 (The MathWorks, Inc.).

Statistical Analysis

To understand relationships between state variables and rates we employed several statistical techniques: ANOVA, Kruskal Wallis (when ANOVA assumptions failed), Spearman Rank, and Random Forest regression. To characterize relationships between variables, we used ANOVA for normally distributed data and Kruskal Wallis and Spearman Rank for nonparametric measures of rank correlation using the R packages (R-core Team, 2019) "Tidyverse" (Wickham et al. 2019) and "Hmisc" (Harrell, 2014). We used Random Forest modeling to characterize variable importance in constraining the variance of rate measurements. Random forest modeling, a machine-learning statistical method which combines many classification trees to produce a more accurate classification (Breiman 2001, Cutler et al. 2007) and has been found to be a robust tool for interpreting ecological datasets (Prasad et al. 2006, Cutler et al. 2007). Random forests provide several metrics that aid in interpretation of multivariable datasets. Variable importance can be evaluated based on how much worse the prediction would be if the data for that predictor were permuted randomly. The resulting tables can be used to compare relative importance among predictor variables (Prasad et al. 2006). Random Forests were conducted using the R package "randomForest" (Law and Weiner 2012).

Results

Wastewater Effluent Characterization

Throughout the study, the effluent nutrient concentrations, isotope ratios, and discharge rates at each outfall were slightly variable (Table 2). Over the study period, both agencies' effluent discharge rate decreased slightly, a part of a long-term trend related to increasing water use efficiency and reduced water consumption in California. During this same time, LACSD discharged an average of 4.1×10^7 ($\pm 4.5 \times 10^6$) grams of inorganic nitrogen per day and OCSD an average of 1.5×10^7 ($\pm 3.2 \times 10^6$) grams of inorganic nitrogen per day. The characteristics of effluent from OCSD and LACSD were different, likely due to differences in their treatment systems. OCSD wastewater treatment is secondary with advanced nitrification/denitrification (NDN) and LACSD is secondary treatment with no advanced nutrient removal. Ammonium accounted for >99% of LACSD's dissolved inorganic nitrogen

(DIN) load and between 55 and 67% of OCSD's DIN load. OCSD's effluent contains more phosphate compared to LACSD, with an average N:P molar ratio of 100:1 for OCSD and 678:1 for LACSD (Table 2). Dissolved inorganic carbon and dissolved organic carbon were highly variable in both agencies' effluent throughout the study period. The stable N isotopic composition of ammonium ($\delta^{15}N_{NH4}$) and nitrate+nitrite ($\delta^{15}N_{NO2+NO3}$) were different for both plants. OCSD had relatively consistent $\delta^{15}N_{NH4}$, with values ranging between 8.6 and 9.1 ‰ and $\delta^{15}N_{NO2+NO3,}$ with values ranging between 7.5 and 9.1 ‰. LACSD had $\delta^{15}N_{NH4}$ values ranging from 5.1 to 12.4 ‰. The ammonium isotopic composition in LACSD's effluent was linearly related to the concentration of ammonium in the wastewater (R^2 for LACSD is 0.907, P = 0.049, and R^2 for OCSD is 0.364, P = 0.505). LACSD also had variable $\delta^{15}N_{NO2+NO3,}$ with values ranging between -9.6 and -2.3 ‰.

Seasonal Hydrography, Chlorophyll, and Dissolved Oxygen

There were clear seasonal differences in temperature and salinity throughout the study region (Figures 2, SI.2). Summer surveys were characterized by high surface water temperatures, shallow thermoclines and haloclines (~10-15 m) and large vertical temperature gradients, indicating strong thermal stratification. Spring surveys were characterized by weaker vertical thermal gradients and deeper thermoclines and haloclines (~20-30 m). The wastewater plume was identifiable by both low salinity and high CDOM in both LACSD's and OCSD's nearfield sub-regions at mid-depth. During Spring 2016 there was a cold, high salinity, low DO water mass intruding into the region from depth throughout the Palos Verdes Shelf region, and notably in the OC Offshore station (CALCOFI station 9030).

There were no statistically significant differences between DO in nearfield versus far field areas (Kruskal Wallis). Nearfield stations generally had shallower oxyclines compared to the farfield stations, but that is likely due to close proximity to shore compared to most farfield stations, except for CP1 (Figure 2). DO profiles varied seasonally (Figures 2, SI.2). In the Summer, all regions had similar profiles and a narrower range of values in the upper 60 m. During the Spring surveys, DO had a larger range of values in the upper 60 meters, with surface ocean values similar to Summer, but much lower at depth. Spring also had greater variability in

the depth to the oxycline among different stations. The lowest DO was in deeper waters and shoaled closer to the surface during Spring (particularly Spring 2016), indicative of upwelling of cold, deep waters, low in DO.

Chlorophyll fluorescence in nearfield areas was slightly, but significantly, higher in nearfield areas compared to farfield within the first 60 m of the water column, which captures the chlorophyll maximum depth at all stations, with a mean chlorophyll *a* concentration of 2 $\mu g\ L^{-1}$ in the nearfield compared to 1 $\mu g\ L^{-1}$ in the farfield ($P < 2e^{-16}$). Daytime, chlorophyll florescence had a similar vertical structure to DO, with a clear subsurface maximum layer in all seasons (Figure 2). The depth to and magnitude of the subsurface chlorophyll maximum was variable among stations and among seasons. The lowest chlorophyll was during Summer 2015 and the highest during Spring 2015. The highest values during Spring 2015 were associated with the LACSD and OCSD nearfield areas, appearing as a thin subsurface chlorophyll layer (Figure 2). Spring 2016 had a shallow, narrow chlorophyll layer, with no chlorophyll fluorescence associated with the deep, salty water mass present in Spring 2016. Summer 2014 had middling water column chlorophyll that was deeper offshore and shallower nearshore, whereas Summer 2015 had relatively low chlorophyll overall with the most consistency among stations.

Sampling occurred over a four-week period for each season and this may have introduced some variability among stations; however, there was no clear pattern within any sampling season of the nearfield stations having consistently different hydrographic conditions relative to the farfield stations that might create bias in the dataset (Figure SI.2).

Water Column Nutrient Concentrations

Dissolved Inorganic Nutrients. Despite the continuous N-load from both wastewater treatment plants, surface dissolved inorganic nitrogen (DIN) concentrations were generally low in all subregions (Figure 3), but not completely depleted. Surface DIN values ranged from not-detected to 26.9 µM with a mean value of 3.6 µM in farfield areas and 4.7 µM in nearfield areas. Nutrient profiles generally showed lower concentrations in surface waters with increasing concentrations at depth (Figure 3). Mean DIN concentrations for samples collected

below the thermocline ranged from 0.6 to 53.9 µM, with a mean value of 18.7 µM in farfield areas and 17.0 µM in nearfield areas). Excluding the bottom sample (which was collected at significantly greater depths offshore compared to the nearshore sites), ammonium and nitrite were significantly higher in the nearfield stations compared to farfield, non-plume stations (P-values of 0.000542 and $1.30e^{-5}$, respectively). High concentrations of ammonium (maximum value of 18.8 µM and a mean value of 5 µM) and nitrite (maximum value of 1.1 µM and mean value of 0.4 µM) were associated with the plume mixing zone (as detected by CDOM, Figure SI.1) in the nearfield regions, the depth where the plume reaches neutral buoyancy in the water column (between 20 and 60 m depth). Nitrate and phosphate were not significantly different in the nearfield compared to the farfield. All dissolved inorganic nutrients showed significant differences by season ($P = 3.86e^{-6}$ for nitrate, $P = 7.69e^{-05}$ for ammonium, and $P = 1.03e^{-10}$ for phosphate), except for nitrite (P = 0.15).

Suspended Particulate Nutrients. Water column suspended particulate nutrients had similar profiles, with the highest concentrations at the surface and decreasing with depth (Figure SI.3). Mean surface particulate nitrogen was 3.5 µM at the surface and 2.5 µM below the thermocline, mean surface particulate phosphorus was 0.18 µM at the surface and 0.12 µM below the thermocline, and mean surface particulate carbon was 19.0 µM and 13.2 µM below the thermocline. There were no statistically significant differences by station type for particulate nitrogen or phosphate, but particulate carbon was slightly, significantly higher in nearfield stations (Kruskal Wallis, P = 0.03), particularly those within the plume mixing zone detected by CDOM (with particulate carbon concentrations 21 µM for depths within the plume in nearfield stations compared to 16.9 µM for similar depths in farfield stations). There were also significant differences by season for all particulate parameters (Kruskal Wallis, P = 0.0008, 0.02, $2.2e^{-16}$, for PC, PN and PP respectively). Spring 2016 was slightly anomalous from the other three seasons, exhibiting higher concentrations in particulate carbon, nitrogen and phosphorus in surface samples relative to the other seasons, perhaps related to the cold, salty water mass intrusion during that season.

Nutrient Ratios. Nutrient concentrations for particulate matter and dissolved inorganic nutrients were highly correlated, following the Redfield relationship of C:N:P 106:16:1 (Figure 4, Figure SI. 4). The mean N:P ratio for dissolved nutrients was 15.4 and was significantly lower ($P = 0.028$) in the farfield (mean DIN:P of 13.4) compared to the nearfield (mean DIN:P of 17.5). The highest mean DIN:P ratios were in the nearfield stations at depths associated with the plume (mean DIN:P of 18.5). The lowest mean DIN:P ratios were recorded at the chlorophyll maximum depth in the farfield (9.9). N* showed strong seasonality, with water column values close to 0 during the Spring upwelling periods, whereas the Summer fluctuated between positive N* values (Summer 2014), indicative of a source of nitrate, and negative N* values (Summer 2015), indicative of a sink for nitrate (Figure 5, Figure SI. 5). N* values near zero suggest that there were no large sources of nitrate (e.g., from nitrogen fixation) or sinks (e.g., due to denitrification).

Particulate matter, particulate C and N were highly correlated, with 90% of C:N ratios between 3.8 and 20.0, with a mean regional C:N of 6.7. There were some differences between particulate C:N ratios in the nearfield and farfield (with mean values of 7.1 and 6.3, respectively). C:N ratios less than 6 were found throughout the water column and are atypical of phytoplankton and often associated with bacteria (Goldman et al. 1987). C:P and N:P relationships were close to Redfield, with occasional deviations. These deviations were not related to depth (Figure SI.4) and were more closely tied to station type, with nearshore stations (nearfield stations and farfield, coastal stations at Camp Pendleton) having greater variability than farfield, offshore stations. Relatively high particulate P concentrations were not matched by high concentrations in N and C during Spring 2016.

Water Column Isotope Ratios

Stable Isotopic Composition of Dissolved Nitrate. $\delta^{15}N_{NO2+NO3}$ values were generally lower in surface waters (mean of 7.5 ‰), increased to a subsurface maximum (mean of 9.5 ‰), before decreasing again (to mean of 8.7 ‰). $\delta^{15}N_{NO2+NO3}$ was significantly higher in the farfield, non-plume stations compared to nearfield stations ($P = 0.02$). The $\delta^{18}O_{NO2+NO3}$ was highest in surface waters (mean of 14.6 ‰) and decreased with depth (mean of 5.2 ‰) with

no obvious maximum or minimum (Figure 6). The shapes of profiles for both $\delta^{15}N_{NO2+NO3}$ and $\delta^{18}O_{NO2+NO3}$ were correlated with the vertical distribution of nitrate, DO, and chlorophyll. There were also significant differences in $\delta^{15}N_{NO2+NO3}$ and $\delta^{18}O_{NO2+NO3}$ values between sampling seasons (P-values of $3.07e^{-10}$ and $6.99e^{-9}$, respectively).

At low nitrate concentrations $\delta^{15}N_{NO2+NO3}$ values were variable, but asymptote towards values between 7 and 9 ‰ for all sampling periods as the concentration of nitrate, the fraction of nitrate in the DIN pool, and as nitrification rate all increase (Figure 5, Figure SI.5), similar to what has been seen in urban coastal environments (Sugimoto et al. 2009, McLaughlin et al. 2017). There was no significant relationship between $\delta^{15}N_{NO2+NO3}$ and N*, largely because N* was typically very close to 0 for most sampling stations and events (Figure 5B, Figure SI.5).

Stable Isotopic Composition of Suspended Particulate Matter. The stable isotopic composition of suspended particulate organic carbon ($\delta^{13}C_{PM}$) and particulate organic nitrogen ($\delta^{15}N_{PM}$) were lower at the surface (-25.9 ‰ and 4.6 ‰, respectively), increased to a subsurface maximum (-25.5 ‰ and 5.4 ‰, respectively), and decreased at depth (-27.2 ‰ and 4.2 ‰, respectively; Figure 6, Figure SI.6). Both $\delta^{13}C_{PM}$ and $\delta^{15}N_{PM}$ were significantly higher in the nearfield areas relative to the farfield ($P = 1.68e^{-06}$ and 0.00107, respectively). There were also significant temporal differences in $\delta^{13}C_{PM}$ and $\delta^{15}N_{PM}$ ($P = < 2e^{-16}$ and $P = 8.22e^{-06}$, respectively). $\delta^{13}C_{PM}$ in Summer 2014 (mean value of -26.7 ‰) and Spring 2015 (-28.9 ‰) were lower than Summer 2015 (-26.0 ‰) and Spring 2016 (-23.8 ‰) and $\delta^{15}N_{PM}$ was highest in Spring 2015 (mean 5.7 ‰), and lowest in Spring 2016 (3.4 ‰), with both summer periods having similar mean values, Summer 2014 (4.4 ‰) and Summer 2015 (4.9 ‰) (Figure 6, Figure SI.6). $\delta^{15}N_{PM}$ showed an asymptote to values between 4 and 10 ‰ with increasing particulate N concentration and chlorophyll *a* concentration (Figure 5I, Figure SI.7). By contrast, no significant relationship between $\delta^{15}N_{PM}$ and particulate N nor $\delta^{15}N_{NO2+NO3}$ was observed (Figure 5G,H, Figure SI.7). $\delta^{13}C_{PM}$ was also positively correlated with $\delta^{15}N_{PM}$ for most stations and seasons and showed an asymptote between -26 and -20 ‰ with increasing particulate carbon concentration and chlorophyll *a* (Figure 5F, Figure SI.8). $\delta^{13}C_{PM}$ was also negatively correlated with water column DIN (Figure SI.8).

Primary Production and Respiration

There was large spatial/temporal variability in both primary production and respiration rates (Figure 7A and 7B, Figure SI.9). Primary production rates ranged from 129 to 2842 mg C m^{-2} d^{-1} and respiration rates ranged from 80.55 to 1521 mg O m^{-3} d^{-1}. There was seasonality in primary production for the two farfield offshore stations, with higher production during the Spring, due to upwelling. However, for the nearshore stations (nearfield stations and the farfield, coastal stations at Camp Pendleton), there were no statistically significant differences between station type (nearfield vs farfield) or season in primary production. Similarly, respiration rates offshore were typically higher than nearshore values, but there were no significant differences between the nearfield stations and farfield, coastal stations (Figure 7B). Primary productivity values were similar to what has been reported for the region (Smith et al. 1982, Eppley 1992) with similar seasonality (Mantyla et al. 2008). Respiration rates are within the range of other coastal areas and slightly higher than what has been reported for the Pacific coastal environment (Robinson 2019). There were no significant differences between the LACSD nearfield and the OCSD nearfield (Figure SI.9). There was no significant relationship between primary production and respiration for any season (Figure SI.10). It should be noted that one integrated rate for both primary production and respiration was provided per station, so sample sizes were small (n = 12 nearfield and farfield sites, 24 total primary production rate estimates; n = 16 nearfield and farfield sites, 32 total respiration rate estimates).

Nitrification

Nitrification rates were highly variable throughout the study ranging from 0.001 to 325 nmol L^{-1} day^{-1}, with no clear seasonal patterns. Rates were significantly higher in samples collected below the thermocline (mean rate of 40.0 nmol L^{-1} day^{-1}) compared to samples collected in the mixed layer (16.5 nmol L^{-1} day^{-1}) and deep chlorophyll *a* maximum (24.6 nmol L^{-1} day^{-1}) ($P = 0.01$; Figure 7C), similar to profiles measured by others (Ward 1987, 2005, Santoro et al. 2010, Smith et al. 2014) and attributed to light inhibition of nitrification in surface waters. Rates were highest in nearshore stations (mean rate of 35.2 nmol L^{-1} day^{-1} in the nearfield stations and the farfield, coastal stations at Camp Pendleton) compared to the

two offshore stations (mean rate of 21.1 nmol L^{-1} day^{-1} offshore) and were significantly higher in nearfield areas (36.2 nmol L^{-1} day^{-1}) relative to farfield areas (23.6 nmol L^{-1} day^{-1}) ($P = 0.04$). There were no significant differences between LACSD and OCSD nearfield stations (Figure SI.9).

Discussion

Anthropogenic nutrient discharges into coastal waters can drive significant biogeochemical changes and local managers are being urged to consider whether nutrient management strategies can slow the progression of acidification and deoxygenation and their impact on coastal habitats (Kelly et al. 2011, Strong et al. 2014, Chan et al. 2016). Globally, wastewater discharge, 80% of which is untreated (WWAP 2017), represents a significant pathway of nutrient enrichment and eutrophication of coastal waters. However, the relative impact of these inputs compared to global change on N and C biogeochemical cycling is poorly characterized (Kelly et al. 2011, Strong et al. 2014), particularly in EBUS. In this study, we document that wastewater nutrient inputs may have an immediate, local effect on nutrient stoichiometry, elevating ammonium and nitrite concentrations and increasing dissolved nitrogen: phosphorus ratios, as well as increasing rates of nitrification within the plume and slightly increasing chlorophyll *a* concentrations. We did not observe a consistent, near plume effect on primary production, respiration, or DO, suggesting any potential impact from wastewater on these processes might be moderated by regional factors, notably mixing of water. Furthermore, a regional assessment of aragonite saturation state conducted at the same time as this study, indicated that there was no clear pattern in reduced Ω_{Ar} near ocean outfalls (McLaughlin et al. 2018). This suggests that further study of implications of these changes on the SCB lower trophic ecosystem through ocean numerical modeling studies is warranted, given the difficulty in disentangling local versus regional versus global drivers through observations alone.

Anthropogenic nutrient inputs impact the biogeochemical cycling of nitrogen in the immediate, local vicinity of outfalls.

The doubling of coastal ocean annual nitrogen loads from wastewater outfalls (Howard et al. 2014) has important implications for nitrogen cycling in the nearshore. Wastewater nitrogen appears to be altering the composition of the N pool within the plumes; ammonium and nitrite concentrations were elevated in the nearfield regions compared to farfield regions (Figure 3). Furthermore, there was no seasonal difference in nitrite concentration, suggesting a source of nitrite independent of seasonal upwelling.

The N:P ratio in coastal waters also appears to be altered by the presence of wastewater plumes. The ratio of N:P is a nearly constant 16:1 throughout the world's oceans, in both plankton biomass and in dissolved nutrient pools (Redfield 1958), and the farfield stations adhere closely to this ratio (Figure 4). However, the nearfield stations had elevated N:P ratios, which can be attributed to the relatively low concentrations of P compared to N in wastewater (Table 2, effluent N:P ~115:1). This increase in P-limitation near outfalls may have important implications for the planktonic community compositions near these discharges (Grosse et al. 2017, Moreno and Martiny 2018, Fagan et al. 2019). For example, harmful algal bloom species (HABs), as P-limitation has been linked to increased toxin production in *Pseudo-nitzschia* (Fehling et al. 2004), a common HABs species in the SCB (Schnetzer et al. 2007b).

Nitrification of ammonium to nitrate has been found to play an important role in coastal ocean nitrogen cycling (Ward 1987, 2005) and can support a significant fraction of productivity in surface waters (Wankel et al. 2007, Santoro et al. 2010). Nitrification rates were significantly higher in nearfield stations compared to farfield areas, suggesting the ammonia from wastewaters may be increasing these rates within the plumes. Though it should be noted that the high concentrations of ammonium in the nearfield and the relatively small percentage of labeled ammonium added to these samples during the incubation experiments (less than 1% spike) may have resulted in an underestimation of nitrification in the nearfield samples. Therefore, the differences in nitrification rates in the nearfield compared to the farfield may be greater than what is described here. Offshore (farfield) rates were consistent with those measured in similar locations in the Southern California Bight (Ward 1987) and coastal

locations in Monterey Bay, California (Ward 2005, Smith et al. 2014), but slightly lower than those measured within the California Current (Santoro et al. 2010). The rate of nitrification is light inhibited and related to ammonium concentration (Ward 2008). Our results are consistent with this, where nitrification rates show positive correlations with water column N species and negative correlations with DO, temperature (Spearman rank analysis, Table 3). Random forest regressions explained a relatively low percent of the variance for nitrification rates, 20% (Figure SI.10). Phosphate and station type, were most predictive, followed by temperature, nitrate and dissolved oxygen, likely related to the fact that nitrifying bacteria are typically light inhibited and thus more abundant below the eutrophic zone, where water temperatures were colder and dissolved oxygen is lower (Ward 1987, 2005, Santoro et al. 2010, Smith et al. 2014). The low percentage of the variability explained by the random forest models suggests that there were other factors which affect the nitrification rates, such as the composition of the bacterial community (Ward 2005) or possibly the added uncertainty of the underestimation of the rates due to insufficient spike as described above.

Wastewater N is predominantly ammonium and is discharged at depth, rising in a buoyant plume and generally trapped below the mixed layer (Figure 3) (Nezlin et al. 2020). Because wastewater ammonium is discharged at depth below the photic zone, wastewater ammonium was expected to be rapidly nitrified. Indeed, elevated nitrite concentrations and higher nitrification rates were associated with OCSD's effluent plume (McLaughlin et al. 2017), and effluent discharges in other coastal regions have seen similarly elevated nitrification rates in sediments near outfalls (Axelrad et al. 1981, Nowicki 1994). Furthermore, the OCSD diversion study was able to track changes in nitrification rates when the plume is "turned-off" relative to "turned-on" and results suggested that wastewater ammonium was nitrified on relatively short time scales; hours to days (McLaughlin et al. 2017). Thus, the contribution of nitrate from the nitrification of wastewater effluent has the potential to support significant productivity in coastal areas. Ammonium concentrations were elevated in nearfield stations relative to farfield stations, particularly at the depths associated with the plume (Figure 3). These high ammonium concentrations were associated with increased nitrification rates, both directly over the outfall and at a distance from the outfall but still within the plume, suggesting

a local impact on N cycling from wastewater effluent discharges. Generally, LACSD's nitrification rates were higher than OCSD's, particularly below the thermocline, which is consistent with the higher concentrations of ammonium in effluent (Figure SI.9). However, OCSD had much greater variability in nitrification rates near its outfall compared to LACSD, with relatively high nitrification rates within the chlorophyll maximum and within the mixed layer, as well as the highest recorded nitrification rate in a bottom sample during Spring 2015, demonstrating the variability present in the rates both within a site and across the region. Concentrations of nitrite, likely from oxidation of ammonium, were elevated within the plume over both outfalls and, as noted above, did not show any seasonal variability suggesting a continuous source (Figure 3). Nitrate concentrations were not significantly elevated in the nearfield relative to farfield stations; however, the concentrations of nitrate were 2-3 times higher than ammonium and 10 times higher than nitrite, thus the additional contribution from nitrification if diluted over a larger area may not have been distinguishable from local heterogeneity in concentrations. Nitrification rates were not higher in the "fresh" plume compared to "older" plume stations, suggesting that the time-scales of nitrification of plume ammonium were on the order of days and that the elevation in nitrification rates encompasses, at minimum, plume areas as defined by this study (i.e., detectable by CDOM).

Regional factors play a more important role in nitrate assimilation compared to localized impacts of wastewater plume.

Nitrate assimilation (incorporation of nitrate into the biomass) was not directly measured in this study; however, stable isotopes were employed as tracers of this process in the water column. The relationship between $\delta^{15}N_{NO2+NO3}$ and $\delta^{18}O_{NO2+NO3}$ was generally consistent with nitrate assimilation in the water column and was not significantly different between seasons and station location. The relative enrichments in $\delta^{15}N_{NO2+NO3}$ and $\delta^{18}O_{NO2+NO3}$ generally fell along a line with a slope of 1 (Figure 5C, Figure SI.5), particularly during the Spring 2016 event; however, the low surface values in $\delta^{15}N_{NO2+NO3}$ resulted in poor or negative correlation between $\delta^{15}N_{NO2+NO3}$ and $\delta^{18}O_{NO2+NO3}$ for some stations. A linear relationship between $\delta^{15}N_{NO2+NO3}$ and $\delta^{18}O_{NO2+NO3}$ with a slope of 1 would be predicted if phytoplankton

assimilation or denitrification were the dominant processes controlling the isotopic composition of nitrate (Granger et al. 2004). However, because concentrations of oxygen were relatively high (always greater than 2 mg L^{-1}), denitrification is not likely to be a significant process in these waters and the isotope affect is likely to be attributed to assimilation (Wankel et al. 2007). It should be noted that because our dissolved nitrate+nitrite oxygen isotope ratios were measured using the denitrifier method, there may be some errors in the apparent $\delta^{18}O_{NO2+NO3}$ values reported. Casciotti et al. (2007) noted that when nitrite was 2% or more of the total nitrate plus nitrite present in the sample, the denitrifier method would give a detectable error in the apparent $\delta^{18}O_{NO2+NO3}$ in the sample, underestimating the value. This is a concern for 30% of our samples, particularly the nearfield stations (38%) where mean nitrite fraction of the nitrate+nitrite pool is 3.8%, though it also affects 20% of the farfield stations where the mean nitrite fraction of 1.2%. This effect only applies to the oxygen isotope values and, assuming the offset would add 25‰ to the $\delta^{18}O$ of nitrite (as estimated by Cassioti et al. 2007) would increase $\delta^{18}O_{NO2+NO3}$ values of samples 0.08 - 13.8‰ with a mean increase of 2.69 ‰, which would slightly reduce the spread of samples along the $\delta^{18}O_{NO2+NO3}$ axis of Figure 5C (Figure SI.12).

As indicated by patterns in $\delta^{15}N_{NO2+NO3}$ and $\delta^{18}O_{NO2+NO3}$, nitrate+nitrite assimilation was not significantly different in nearfield areas versus farfield areas, but had clear seasonal patterns, suggesting regional mixing and dilution of wastewater N likely spreads the impact on assimilation over a much wider area thereby creating a potential temporal lag in effect. During upwelling periods, particularly during the Spring of 2016, the effect of assimilation on the isotopic composition of the dissolved nitrate pool is evident from the measurements of $\delta^{18}O_{NO2+NO3}$ and falling along a 1:1 line (Figure 5C, Figure SI.5). However, during the Summer sampling periods, the isotope effect from assimilation of “new” nitrate from upwelling is diluted and the relationship between the two isotopes appears more influenced by nitrification (low $\delta^{15}N_{NO2+NO3}$ and high $\delta^{18}O_{NO2+NO3}$). In Monterey Bay, in northern California, nitrification of “natural” ammonium from regenerated organic matter was found to contribute ~30% of nitrate based primary production (Wankel et al. 2007). The isotopic composition of dissolved nitrate at all stations increased with nitrate concentration and the fraction of nitrate

in the DIN pool. This is consistent with nitrification as a significant driver defining the composition of the DIN pool and the isotopic composition thereof, region-wide (Sugimoto et al. 2009, McLaughlin et al. 2017). However, because nitrification is largely happening below the euphotic zone, the importance of this source for regional primary productivity will be directly related to physical mixing in the region. Time scales of when this subsurface nitrate source mixes into the surface waters could result in impacts of this source in the farfield regions and not necessarily near the discharge location.

Impacts of anthropogenic nutrient inputs on the biogeochemical cycling of carbon and oxygen are regional in scale.

Regional factors such as upwelling and Pacific Basin-scale changes in circulation have been shown to be the primary drivers for the concentrations of chlorophyll biomass and the depth of the chlorophyll maximum layer (Mantyla et al. 2008, Nezlin et al. 2012, Nezlin et al. 2018). This work highlights the importance of regional-scale influences on carbon and oxygen cycling. In this study, no statistically significant differences in instantaneous rates of primary productivity and respiration were found in nearfield areas versus farfield (Figure 7). This is consistent with an investigation of pH and aragonite saturation state during the same time period as this study, which found no significant differences between these parameters on the continental shelf (near anthropogenic discharges) compared to offshore of these influences (McLaughlin et al. 2018). While there were some regional differences in chlorophyll *a* and dissolved oxygen, and mean chlorophyll fluorescence was increased in proximity to the wastewater plume, there was a high amount of variability among stations and seasons (Figure 2, Table 3). This is consistent with other research in the area which has shown that physical mixing processes, such as internal waves which can create thin bands of high productivity along the coast and have a significant effect on primary production over relatively small spatial scales (Lucas et al. 2011, Omand et al. 2011, 2012). The alteration of the N:P ratios in nearfield regions could impact phytoplankton community productivity as noted above (Grosse et al. 2017, Moreno and Martiny 2018, Fagan et al. 2019), resulting in a dilution of the impact of increased N over a larger area. Furthermore, we saw evidence of seasonal upwelling bringing

increased chlorophyll biomass and intrusions of deep, cold waters that are low in dissolved oxygen into surface waters; impacting both nearfield and farfield regions. This supports the hypothesis that regional mixing of water masses dilutes the impact of wastewater N on the coastal environment, potentially enhanced by outfall diffuser systems which discharge effluent over large areas, spreading the effect on primary production and respiration over larger areas, and by extension carbon and oxygen cycling in the SCB (Mantyla et al. 2008, Nezlin et al. 2012, Nezlin et al. 2018).

Random forest regression characterized a low percent of variance for both primary production and respiration (30% and 18%, respectively Figure SI.11), thus the primary drivers for variability in these processes were either not well accounted for in the observed parameters or the relationships between factors are diluted regionally. Season was the most predictive variable of primary production in random forest analysis, indicating the importance of regional variables on primary productivity, as the SCB is subject to seasonal upwelling. This is shown in the seasonal differences in temperature, salinity and chlorophyll *a* during the study (Figure 2). Station type was not very predictive for either primary production or respiration, suggesting any impact of the wastewater plume is diluted across the region. This dilution effect is also apparent in the isotopic signature of the assimilation of "new" nitrate on $\delta^{15}N_{NO2+NO3}$ is also mixed throughout the study area, particularly during Summer, stratified, periods (Figure 5C). Furthermore, concentrations of suspended particulate matter (carbon, nitrogen and phosphorus) and nutrient ratios within that suspended matter were not significantly different in the nearfield versus the farfield (Figures 4 and 5). This decoupling of the presence of the wastewater plume, and its associated nutrients, from primary production, suspended organic matter, and respiration can be explained by regional dilution of effluent nitrogen due to water mass mixing. Both LACSD and OCSD outfalls have multiport diffusers to disperse and increase dilution of the plume over a large area to minimize immediate local impacts of the discharge on the coastal ocean environment (Koh and Brooks 1975). The relative buoyancy of the plume to local seawater traps the plume in the subsurface near the base of the euphotic zone where nutrients could be utilized by primary producers, but the impact is designed to be diluted over a larger area dictated by the local hydrodynamics of

plume mixing as well as seasonal, basin-scale changes in currents and ocean state. Given that no difference was observed in primary production and respiration in plume affected areas relative to farfield areas, it is likely that effect of effluent nutrients on these processes are either diluted throughout the region into farfield areas or is too small to detect.

While most of the patterns in carbon and oxygen cycling were regional in scope, there was some evidence of local influence. Isotopic signatures of particulate matter ($\delta^{15}N_{PM}$ and $\delta^{13}C_{PM}$) were both slightly, but significantly higher the nearfield compared to farfield, potentially reflecting a small local influence on carbon and nitrogen cycling (Figure 5). Higher $\delta^{15}N_{PM}$ and $\delta^{13}C_{PM}$ have been associated with higher primary productivity in coastal areas (Oczkowski et al. 2014, 2016) and may be a more integrated metric of primary productivity differences than an instantaneous rate measurement. The isotopic composition of nitrogen in suspended material ($\delta^{15}N_{PM}$) is slightly lower than dissolved nitrate in the water column ($\delta^{15}N_{NO2+NO3}$) indicating the presence of a small isotopic discrimination associated with uptake of nitrate into the biomass (Figure 5H) (Ostrom et al. 1997). The lighter isotope is preferentially utilized by phytoplankton and, as N becomes limiting, this isotopic discrimination becomes less and less until the isotopic composition of the biomass is the same as that of the N being utilized (Ostrom et al. 1997), as such higher values are typically associated with more competition for N and higher primary production (Oczkowski et al. 2014, 2016). Both $\delta^{15}N_{PM}$ and $\delta^{13}C_{PM}$ increased with chlorophyll fluorescence (Figure 5I, F). Using chlorophyll *a* as a proxy for phytoplankton biomass, an increase in $\delta^{13}C_{PM}$ with biomass is consistent with lowering of dissolved inorganic carbon and dissolved carbon dioxide (Ostrom et al. 1997). Furthermore, chlorophyll *a* fluorescence was also slightly significantly higher in the nearfield, which may reflect increased biomass in the nearshore. This has important implications for regional variability in acidification. Nutrient enrichment of coastal waters has been linked to impacts on the aragonite saturation state, inducing waters into undersaturated conditions when they otherwise might not have been (Cai et al. 2011, Wallace et al. 2014, Rheuban et al. 2019). Regionally, the SCB is exposed to waters with aragonite saturations states below thresholds thought to be important for marine calcifers (McLaughlin et al. 2018), and further investigation

into potential enhancement of acidification associated with increased primary production is therefore warranted.

The failings of a "reference-area" approach to document impacts of point sources on nutrient and carbon cycling.

The study design was based upon the hypothesis that areas near wastewater outfalls would be more impacted from nutrient discharges than areas spatially distant from the outfalls. Results suggest that such a concept is has limitations. While nitrification, which occurs at depths directly associated with detectable plume, showed significant differences between nearfield and farfield stations, instantaneous rates of primary production and respiration, an immediate, local effect was not observed. While a slight lag in the timing (and thus distance) of elevated primary production and chlorophyll *a* from wastewater N discharged by ocean outfalls at depth was expected, the observations suggest that levels of advection, stirring, and eventual mixing in the region were sufficient to transport anthropogenic nutrients to presumed "minimally disturbed" reference areas in the farfield. Thus, the concept of a "reference area" (Nezlin et al., 2020) as implemented here in the SCB is flawed for nutrient impacts on these processes. This is supported by numerical ocean model simulations from the Regional Ocean Modeling System (ROMS,www.myroms.org; (Shchepetkin and McWilliams 2005)) run in particle tracking mode to track Lagrangian flow of "plume particles" (Figure 8). When particles were released from the outfalls, they were transported to farfield areas used for this study on timescales of weeks to months, suggesting that wastewater N is mixed over larger regional scales. In such cases, impacts of anthropogenic nutrients on primary production, related elevation in respiration, and impacts on carbon cycling/acidification, are not easily deciphered with observational data alone. Thus, the monitoring scheme to assess nutrient impacts should be reevaluated to include modeling approaches that can account for the complexity of mixing and farfield transport in the region.

Conclusion

In this study, we found that wastewater nutrient inputs have an immediate, local effect on nutrient stoichiometry and nitrogen concentrations and elevated rates of nitrification within the plume. Impact of wastewater plumes on nitrate assimilation, primary production, chlorophyll *a*, respiration, and DO was moderated by regional mixing of water masses. This lends strong support for further study of local anthropogenic forcing through ocean numerical modeling studies, given the difficulty of disentangling local to global scale drivers through observations alone (Chan et al. 2016). While observational studies such as this are costly, they provide key data needed to evaluate ocean numerical models. These data should not only include state variables, which can be used to characterize the uncertainty in model output (is the model getting the right answers), but also rate variables, which can be used to determine if the model configuration accurately represents the underlying biogeochemical processes creating that output (is the model getting the right answers for the right reasons).

References

Anderson, C. R., M. A. Brzezinski, L. Washburn, and R. Kudela. 2006. Circulation and environmental conditions during a toxigenic pseudo-nitzschia australis bloom in the santa barbara channel, california. Marine Ecology Progress Series 327:119-133.

Axelrad, D., G. Poore, G. Arnott, J. Bauld, V. Brown, R. Edwards, and N. Hickman. 1981. The effects of treated sewage discharge on the biota of port phillip bay, victoria, australia. Pages 279-306 Estuaries and nutrients. Springer.

Boesch, D. F. 2019. Barriers and bridges in abating coastal eutrophication. Frontiers in Marine Science 6:123.

Bograd, S. J., C. G. Castro, E. Di Lorenzo, D. M. Palacios, H. Bailey, W. Gilly, and F. P. Chavez. 2008. Oxygen declines and the shoaling of the hypoxic boundary in the california current. . Geophys. Res. Lett. 35:L12607

Booth, J. A. T., C. B. Woodson, M. Sutula, F. Micheli, S. B. Weisberg, S. J. Bograd, A. Steele, J. Schoen, and L. B. Crowder. 2014. Patterns and potential drivers of declining oxygen

content along the southern california coast. Limnology and Oceanography 59:1127-1138.

Borges, A. V. and N. Gypens. 2010. Carbonate chemistry in the coastal zone responds more strongly to eutrophication than to ocean acidification. Limnology and Oceanography 55:346-353.

Breiman, L. 2001. Random forests. Machine learning 45:5-32.

Breitburg, D., L. A. Levin, A. Oschlies, M. Grégoire, F. P. Chavez, D. J. Conley, V. Garçon, D. Gilbert, D. Gutiérrez, and K. Isensee. 2018. Declining oxygen in the global ocean and coastal waters. Science 359.

Brzezinski, M. A. and L. Washburn. 2011. Phytoplankton primary productivity in the santa barbara channel: Effects of wind-driven upwelling and mesoscale eddies. Journal of Geophysical Research: Oceans 116.

Cai, W. J., X. P. Hu, W. J. Huang, M. C. Murrell, J. C. Lehrter, S. E. Lohrenz, W. C. Chou, W. D. Zhai, J. T. Hollibaugh, Y. C. Wang, P. S. Zhao, X. H. Guo, K. Gundersen, M. H. Dai, and G. C. Gong. 2011. Acidification of subsurface coastal waters enhanced by eutrophication. Nature Geoscience 4:766-770.

Capone, D. G. and D. A. Hutchins. 2013. Microbial biogeochemistry of coastal upwelling regimes in a changing ocean. Nature Geoscience 6:711-717.

Casciotti, K.L., Böhlke, J.K., McIlvin, M.R., Mroczkowski, S.J. and Hannon, J.E., 2007. Oxygen isotopes in nitrite: Analysis, calibration, and equilibration. Analytical Chemistry, 79(6), pp.2427-2436.

Casciotti, K. L., D. M. Sigman, M. G. Hastings, J. K. Bohlke, and A. Hilkert. 2002. Measurement of the oxygen isotopic composition of nitrate in seawater and freshwater using the denitrifier method. Analytical Chemistry 74:4905-4912.

Chan, F., A. B. Boehm, J. A. Barth, E. A. Chornesky, A. G. Dickson, R. A. Feely, B. Hales, T. M. Hill, G. Hofmann, D. Ianson, T. Klinger, J. Largier, J. Newton, T. F. Pedersen, G. N. Somero, M. Sutula, W. W. Wakefield, G. G. Waldbusser, S. B. Weisberg, and E. A. Whiteman. 2016. The west coast ocean acidification and hypoxia science panel: Major findings, recommendations, and actions., Oakland, California, USA.

Chavez, F. P. and M. Messié. 2009. A comparison of eastern boundary upwelling ecosystems. Progress in Oceanography 83:80-96.

Cullen, J. and R. Eppley. 1981. Chlorophyll maximum layers of the southern-california bight and possible mechanisms of their formation and maintenance. Oceanologica Acta 4:23-32.

Cutler, D. R., T. C. Edwards, K. H. Beard, A. Cutler, K. T. Hess, J. Gibson, and J. J. Lawler. 2007. Random forests for classification in ecology. Ecology 88:2783-2792.

Dauhajre, D. P., J. C. McWilliams, and L. Renault. 2019. Nearshore lagrangian connectivity: Submesoscale influence and resolution sensitivity. Journal of Geophysical Research: Oceans 124:5180-5204.

Diaz, R.J. and Rosenberg, R., 2008. Spreading dead zones and consequences for marine ecosystems. science, 321(5891), pp.926-929.

Deutsch, C., H. Frenzel, J. C. McWilliams, L. Renault, F. Kessouri, E. Howard, J.-H. Liang, D. Bianchi, and S. Yang. in review. Biogeochemical variability in the california current system. https://doi.org/10.1101/2020.02.10.942565.

Deutsch, C., N. Gruber, R. M. Key, J. L. Sarmiento, and A. Ganachaud. 2001. Denitrification and n-2 fixation in the pacific ocean. Global Biogeochemical Cycles 15:483-506.

Eppley, R. W. 1992. Chlorophyll, photosynthesis and new production in the southern california bight. Progress in oceanography 30:117-150.

Fagan, A. J., A. R. Moreno, and A. C. Martiny. 2019. Role of enso conditions on particulate organic matter concentrations and elemental ratios in the southern california bight. Frontiers in Marine Science 6:386.

Fehling, J., K. Davidson, C. J. Bolch, and S. S. Bates. 2004. Growth and domoic acid production by pseudo-nitzschia seriata (bacillariophyceae) under phosphate and silicate limitation 1. Journal of Phycology 40:674-683.

Fennel, K. and J. M. Testa. 2019. Biogeochemical controls on coastal hypoxia. Annual Review of Marine Science 11:105-130.

Glibert, P. M., J. Harrison, C. Heil, and S. Seitzinger. 2006. Escalating worldwide use of urea - a global change contributing to coastal eutrophication. Biogeochemistry 77:441-463.

Goldman, J. C., D. A. Caron, and M. R. Dennett. 1987. Regulation of gross growth efficiency and ammonium regeneration in bacteria by substrate c-n ratio. Limnology and Oceanography 32:1239-1252.

Grosse, J., A. Burson, M. Stomp, J. Huisman, and H. T. Boschker. 2017. From ecological stoichiometry to biochemical composition: Variation in n and P supply alters key biosynthetic rates in marine phytoplankton. Frontiers in microbiology 8:1299.

Gruber, N. and J. L. Sarmiento. 1997. Global patterns of marine nitrogen fixation and denitrification. Global Biogeochemical Cycles 11:235-266.

Henriksen, K. 1988. Nitrification in estuarine and coastal marine sediments. Nitrogen cycling in coastal marine environments.

Holmes, R. M., A. Aminot, R. Kerouel, B. A. Hooker, and B. J. Peterson. 1999. A simple and precise method for measuring ammonium in marine and freshwater ecosystems. Canadian Journal of Fisheries and Aquatic Sciences 56:1801-1808.

Howard, M. D. A., M. Sutula, D. A. Caron, Y. Chao, J. D. Farrara, H. Frenzel, B. Jones, G. Robertson, K. McLaughlin, and A. Sengupta. 2014. Anthropogenic nutrient sources rival natural sources on small scales in the coastal waters of the southern california bight. Limnology and Oceanography 59:285-297.

Howarth, R. W., A. Sharpley, and D. Walker. 2002. Sources of nutrient pollution to coastal waters in the united states: Implications for achieving coastal water quality goals. Estuaries 25:656-676.

Kelley, D. and C. Richards. 2017. Oce: Analysis of oceanographic data. R package version 0.9-21. Retrieved from https://CRAN.R-project.org/package=oce.

Kelly, R. P., M. Foley, W. Fisher, R. Feely, B. Halpern, G. Waldbusser, and M. Caldwell. 2011. Mitigating local causes of ocean acidification with existing laws. Science 332:1036-1037.

Kessouri, F., McLaughlin, K., Sutula, M.A., Bianchi, D., Ho, M., McWilliams, J.C., Renault, L., Molemaker, J., Deutsch, C.A. and Leinweber, A., 2020. Configuration and validation of an oceanic physical and biogeochemical model to investigate coastal eutrophication: case study in the Southern California Bight.

Koch, S. E., M. desJardins, and P. J. Kocin. 1983. An interactive barnes objective map analysis scheme for use with satellite and conventional data. Journal of Applied Meteorology and Climatology 22:1487-1503.

Koh, R. C. and N. H. Brooks. 1975. Fluid mechanics of waste-water disposal in the ocean. Annual Review of Fluid Mechanics 7:187-211.

Lucas, A.J., Franks, P.J. and Dupont, C.L., 2011. Horizontal internal-tide fluxes support elevated phytoplankton productivity over the inner continental shelf. Limnology and Oceanography: Fluids and Environments, 1(1), pp.56-74.

Mantyla, A. W., S. J. Bograd, and E. L. Venrick. 2008. Patterns and controls of chlorophyll-a and primary productivity cycles in the southern california bight. Journal of Marine Systems 73:48-60.

McLaughlin, K., N. P. Nezlin, M. D. Howard, C. D. Beck, R. M. Kudela, M. J. Mengel, and G. L. Robertson. 2017. Rapid nitrification of wastewater ammonium near coastal ocean outfalls, southern california, USA. Estuarine, Coastal and Shelf Science 186:263-275.

McLaughlin, K., N. P. Nezlin, S. B. Weisberg, A. G. Dickson, J. A. T. Booth, C. L. Cash, A. Feit, J. R. Gully, M. D. Howard, and S. Johnson. 2018. Seasonal patterns in aragonite saturation state on the southern california continental shelf. Continental Shelf Research 167:77-86.

Moreno, A. R. and A. C. Martiny. 2018. Ecological stoichiometry of ocean plankton. Annual Review of Marine Science 10:43-69.

Nezlin, N., M. A. Sutula, R. P. Stumpf, and A. Sengupta. 2012. Phytoplankton blooms detected by seawifs along the central and southern california coast. Journal of Geophsical Research 117:C07004.

Nezlin, N. P., C. Beegan, A. Feit, J. R. Gully, A. Latker, K. McLaughlin, M. J. Mengel, G. L. Robertson, A. Steele, and S. B. Weisberg. 2020. Colored dissolved organic matter (cdom) as a tracer of effluent plumes in the coastal ocean. Regional Studies in Marine Science 35:101163.

Nezlin, N. P., K. McLaughlin, J. A. T. Booth, C. L. Cash, D. W. Diehl, K. A. Davis, A. Feit, R. Goericke, J. R. Gully, and M. D. Howard. 2018. Spatial and temporal patterns of

chlorophyll concentration in the southern california bight. Journal of Geophysical Research: Oceans 123:231-245.

Nowicki, B. L. 1994. The effect of temperature, oxygen, salinity, and nutrient enrichment on estuarine denitrification rates measured with a modified nitrogen gas flux technique. Estuarine, Coastal and Shelf Science 38:137-156.

Oczkowski, A., Kreakie, B., McKinney, R.A. and Prezioso, J., 2016. Patterns in stable isotope values of nitrogen and carbon in particulate matter from the Northwest Atlantic continental shelf, from the Gulf of Maine to Cape Hatteras. *Frontiers in Marine Science*, *3*, P.252.

Oczkowski, A., Markham, E., Hanson, A. and Wigand, C., 2014. Carbon stable isotopes as indicators of coastal eutrophication. *Ecological Applications*, *24*(3), pp.457-466.

Omand, M.M., Feddersen, F., Guza, R.T. and Franks, P.J.S., 2012. Episodic vertical nutrient fluxes and nearshore phytoplankton blooms in Southern California. *Limnology and oceanography*, *57*(6), pp.1673-1688.

Omand, M.M., Leichter, J.J., Franks, P.J., Guza, R.T., Lucas, A.J. and Feddersen, F., 2011. Physical and biological processes underlying the sudden surface appearance of a red tide in the nearshore. *Limnology and Oceanography*, *56*(3), pp.787-801.

Ostrom, N. E., S. A. Macko, D. Deibel, and R. J. Thompson. 1997. Seasonal variation in the stable carbon and nitrogen isotope biogeochemistry of a coastal cold ocean environment. Geochimica et Cosmochimica Acta 61:2929-2942.

Patton, C. and J. R. Kryskalla. 2003. Methods of analysis by the u.S. Geological survey national water quality laboratory—evaluation of alkaline persulfate digestion as an alternative to kjeldahl digestion for determination of total and dissolved nitrogen and phosphorus in water, water-resources investigations report 03–4174. U.S. Department of the Interior, U.S. Geological Survey, Denver, CO.

Powley, H. R., H. H. Dürr, A. T. Lima, M. D. Krom, and P. Van Cappellen. 2016. Direct discharges of domestic wastewater are a major source of phosphorus and nitrogen to the mediterranean sea. Environmental Science & Technology 50:8722-8730.

Prasad, A. M., L. R. Iverson, and A. Liaw. 2006. Newer classification and regression tree techniques: Bagging and random forests for ecological prediction. Ecosystems 9:181-199.

Provoost, P., S. Van Heuven, K. Soetaert, R. Laane, and J. Middelburg. 2010. Seasonal and long-term changes in ph in the dutch coastal zone. Biogeosciences 7:3869.

Rabalais, N. N., W.-J. Cai, J. Carstensen, D. J. Conley, B. Fry, X. Hu, Z. Quinones-Rivera, R. Rosenberg, C. P. Slomp, and R. E. Turner. 2014. Eutrophication-driven deoxygenation in the coastal ocean. Oceanography 27:172-183.

R Core Team. 2019. R: A language and environment for statistical computing. R Foundation for Statistical Computing, Vienna, Austria. URL https://www.R-project.org/.

Redfield, A. C. 1958. The biological control of chemical factors in the environment. American Scientist 46:205-221.

Rheuban, J. E., S. C. Doney, D. C. McCorkle, and R. W. Jakuba. 2019. Quantifying the effects of nutrient enrichment and freshwater mixing on coastal ocean acidification. Journal of Geophysical Research: Oceans.

Robinson, C., 2019. Microbial respiration, the engine of ocean deoxygenation. *Frontiers in Marine Science*, *5*, p.533.

Roberts, P. J., H. J. Salas, F. M. Reiff, M. Libhaber, A. Labbe, and J. C. Thomson. 2010. Marine wastewater outfalls and treatment systems. IWA publishing.

Rogowski, P., E. Terrill, M. P. Otero, L. Hazard, and W. Middleton. 2012. Mapping ocean outfall plumes and their mixing using autonomous underwater vehicles. Journal of Geophysical Research-Oceans 117 1-12.

Rogowski, P., E. Terrill, M. P. Otero, L. Hazard, and W. Middleton. 2013. Ocean outfall plume characterization using an autonomous underwater vehicle. Water Science and Technology 67:925-933.

Santoro, A. E., K. L. Casciotti, and C. A. Francis. 2010. Activity, abundance and diversity of nitrifying archaea and bacteria in the central california current. Environmental Microbiology 12:1989-2006.

Schnetzer, A., B. H. Jones, R. A. Schaffner, I. Cetinic, E. Fitzpatrick, P. E. Miller, E. L. Seubert, and D. A. Caron. 2013. Coastal upwelling linked to toxic pseudo-nitzschia australis blooms in los angeles coastal waters, 20052007. Journal of Plankton Research 35:1080-1092.

Schnetzer, A., P. E. Miller, R. A. Schaffner, B. A. Stauffer, B. H. Jones, S. B. Weisberg, P. M. DiGiacomo, W. M. Berelson, and D. A. Caron. 2007a. Blooms of pseudo-nitzschia and domoic acid in the san pedro channel and los angeles harbor areas of the southern california bight, 2003-2004. Harmful Algae 6:372-387.

Schnetzer, A., P. E. Miller, R. A. Schaffner, B. A. Stauffer, B. H. Jones, S. B. Weisberg, P. M. DiGiacomo, W. M. Berelson, and D. A. Caron. 2007b. Blooms of pseudo-nitzschia and domoic acid in the san pedro channel and los angeles harbor areas of the southern california bight, 2003–2004. Harmful algae 6:372-387.

Shchepetkin, A. F. and J. C. McWilliams. 2005. The regional oceanic modeling system (roms): A split-explicit, free-surface, topography-following-coordinate oceanic model. Ocean modelling 9:347-404.

Sigman, D. M., J. Granger, P. J. DiFiore, M. M. Lehmann, R. Ho, G. Cane, and A. van Geen. 2005. Coupled nitrogen and oxygen isotope measurements of nitrate along the eastern north pacific margin. Global Biogeochemical Cycles 19.

Smith, J. M., K. L. Casciotti, F. P. Chavez, and C. A. Francis. 2014. Differential contributions of archaeal ammonia oxidizer ecotypes to nitrification in coastal surface waters. The ISME journal 8:1704.

Smith, R., R. Eppley, and K. Baker. 1982. Correlation of primary production as measured aboard ship in southern california coastal waters and as estimated from satellite chlorophyll images. Marine Biology 66:281-288.

Smith, J.; Connell, P.; Evans, R. H.; Gellene, A. G.; Howard, M. D. A.; Jones, B. H.; Kaveggia, S.; Palmer, L.; Schnetzer, A.; Seegers, B. N.; Seubert, E. L.; Tatters, A. O.; Caron, D. A., A decade and a half of *Pseudo-nitzschia* spp. and domoic acid along the coast of southern California. *Harmful Algae* 2018, *79*, 87-104.

Strong, A. L., K. J. Kroeker, L. T. Teneva, L. A. Mease, and R. P. Kelly. 2014. Ocean acidification 2.0: Managing our changing coastal ocean chemistry. Bioscience 64:581-592.

Sugimoto, R., A. Kasai, T. Miyajima, and K. Fujita. 2009. Controlling factors of seasonal variation in the nitrogen isotope ratio of nitrate in a eutrophic coastal environment. Estuarine Coastal and Shelf Science 85:231-240.

Sunda, W. G. and W.-J. Cai. 2012. Eutrophication induced co2-acidification of subsurface coastal waters: Interactive effects of temperature, salinity, and atmospheric P co2. Environmental Science & Technology 46:10651-10659.

Sutton, A., R. Wanninkhof, C. Sabine, R. Feely, M. Cronin, and R. Weller. 2017. Variability and trends in surface seawater pco2 and co2 flux in the pacific ocean. Geophysical Research Letters 44:5627-5636.

Sutula, M., A. Sengupta, M. Ho, F. Kessouri, K. McLaughlin, K. McCune, and D. Bianchi. 2020. Southern california bight rivers, wastewater effluents and atmospheric data. https://doi.org/10.5281/zenodo.3981643.

Thomas, W. H., D. L. Seibert, and A. N. Dodson. 1974. Phytoplankton enrichment experiments and bioassays in natural coastal sea water and in sewage outfall receiving waters off southern california. Estuarine and Coastal Marine Science 2:191-206.

Valiela, I., C. Owens, E. Elmstrom, and J. Lloret. 2016. Eutrophication of cape cod estuaries: Effect of decadal changes in global-driven atmospheric and local-scale wastewater nutrient loads. Marine Pollution Bulletin 110:309-315.

Waldbusser, G. G. 2011. The causes of acidification in chesapeake bay and consequences to oyster shell growth and dissolution. Pages 559-560 *in* Journal of Shellfish Research. NATL SHELLFISHERIES ASSOC C/O DR. SANDRA E. SHUMWAY, UNIV CONNECTICUT, 1080 ….

Waldbusser, G. G., H. Bergschneider, and M. A. Green. 2010. Size-dependent ph effect on calcification in post-larval hard clam mercenaria spp. Marine Ecology Progress Series 417:171-182.

Wallace, R. B., H. Baumann, J. S. Grear, R. C. Aller, and C. J. Gobler. 2014. Coastal ocean acidification: The other eutrophication problem. Estuarine, Coastal and Shelf Science 148:1-13.

Wankel, S. D., C. Kendall, C. A. Francis, and A. Paytan. 2006. Nitrogen sources and cycling in the san francisco bay estuary: A nitrate dual isotopic composition approach. Limnology and Oceanography 51:1654-1664.

Wankel, S. D., C. Kendall, J. T. Pennington, F. P. Chavez, and A. Paytan. 2007. Nitrification in the euphotic zone as evidenced by nitrate dual isotopic composition: Observations from monterey bay, california. Global Biogeochemical Cycles 21.

Ward, B. B. 1987. Nitrogen transformations in the southern california bight. Deep-Sea Reseach 34:785-805.

Ward, B. B. 2005. Temporal variability in nitrification rates and related biogeochemical factors in monterey bay, california, USA. Marine Ecology Progess Series 292:97-109.

Ward, B. B. 2008. Nitrification in marine systems.

Wickham, H., M. Averick, J. Bryan, W. Chang, L. D. McGowan, R. François, G.Grolemund, A. Hayes, L. Henry, J. Hester, M.Kuhn, T. Lin, Pedersen, E. Miller, S. M. Bache, K. Müller, J. Ooms, D. Robinson, D.P. Seidel, V. Spinu, K. Takahashi, D. Vaughan, Cl. Wilke, K. Woo, H. Yutani. 2019. Welcome to the tidyverse. Journal of Open Source Software, 4(43), 1686, https://doi.org/10.21105/joss.01686

Wood, I. R., R. G. Bell, and D. L. Wilkinson. 1993. Ocean disposal of wastewater. World Scientific.

Contributions

Karen McLaughlin was the co-lead on this project with Meredith Howard. McLaughlin contributed to study design, led the nutrient and stable isotope analysis and nitrification rates study, conducted the data analysis and drafted the final report.

Meredith D.A. Howard was the co-lead on the project with Karen McLaughlin. She contributed to study design, managed project budget, coordinated the field work and led the primary production and respiration portions of the study. She contributed to primary production and respiration sections of the report and reviewed the final draft.

George Robertson coordinated field sampling with the Sanitation Districts, contributed to study design, reviewed data analysis plan and preliminary data, and reviewed the manuscript on behalf of management agencies.

Carly D.A. Beck was the lead research technician on the project. She contributed to study design, managed field staff in the field and coordinated data collection and quality assurance and reviewed the final report.

Minna Ho is a partner on the modeling effort. She provided the particle tracking model output and interpretation of the observational data.

Fayçal Kessouri is the lead modeler working on nutrient impacts on coastal environments. Kessouri engineered the ROMS model used for particle tracking model output and interpretation of the observational data.

Nikolay P. Nezlin contributed data analysis for the nitrification study and analysis of water column profiles.

Martha Sutula is the Principal Investigator of the Biogeochemistry Department at SCCWRP, she contributed project management, study design, and drafted portions of the final report.

Stephen B. Weisberg is the Executive Director at SCCWRP, he contributed project management, coordination with stakeholders, and reviewed the final draft.

Acknowledgements

The authors thank field sampling and laboratory personnel from the following organizations: City of San Diego, Orange County Sanitation District, Los Angeles County Sanitation Districts, and the Southern California Coastal Water Research Project. We also want to thank members of the Southern California Bight 2013 Regional Marine Monitoring Program Nutrients and Water Quality Committee who contributed thoughtful comments on study design, data analysis and interpretation, and thoughtful comments on early drafts of this manuscript.

Funding Information

Funding for this project was provided from Orange County Sanitation District, Los Angeles County Sanitation Districts, and the Southern California Coastal Water Research Project.

Competing Interests/ Conflicts of Interest

Dr. Martha Sutula is an editor in the Ecology and Earth Systems Domain and the lead author's husband, Dr. Steven Allison, is Editor-in chief for that same Domain.

Data Accessibility

This study was done in collaboration with the Southern California Bight Regional Marine Monitoring Program, a collaborative monitoring program whose goal is to collect regional-scale data on the health of coastal habitats that can be used to make better management decisions. Pursuant to this goal, all data will be made publicly available on SCCWRP's website: www.sccwrp.org

Table 1. Site information.

Station ID	Site Description	Region Category	Periods Sampled	Latitude/ Longitude	Depth (m)
2903	LACSD Ocean Outfall	Nearfield	All	33.698/ -118.336	60
3053	LACSD Off-Outfall (northern current)	Nearfield	Summer 2014	33.730/ -118.402	60
3003	LACSD Off-Outfall (northern current)	Nearfield	Spring 2015	33.757/ -118.441	60
2803	LACSD Off-Outfall (southern current)	Nearfield	Summer 2015 Spring 2016	33.668/ -118.297	60
2602	Long Beach Harbor Shelf (LA County)	Nearfield	All	33.694/ -118.191	23
2205	OCSD Ocean Outfall	Nearfield	All	33.576/ -118.005	57
2306	OCSD Off-Outfall (northern current)	Nearfield	Summer 2014	33.581/ -118.052	114
2103	OCSD Off-Outfall (southern current)	Nearfield	Spring 2015 Summer 2015 Spring 2016	33.585/ -117.945	110
1903	Orange County Southern Transect Line	Nearfield	All	33.546/ -117.836	100
CP1	Camp Pendleton- on shelf	Farfield	All	33.215/ -117.481	65
CP2	Camp Pendleton- continental slope	Farfield	All	33.184/ -117.523	430
SPOTS	San Pedro Ocean Time Series (LA County Offshore)	Farfield	All	33.607/ -118.409	730
90.30	CALCOFI station 90 30 (Orange County Offshore)	Farfield	All	33.419/ -117.912	580

Table 2. Nutrient properties of OCSD and LACSD wastewater effluent. Isotope samples for Aug 2015 and Mar 2016 were not analyzed.

Agency	LACSD					OCSD			
Season	Aug-14	Mar-15	Aug-15	Mar-16		Aug-14	Mar-15	Aug-15	Mar-16
Discharge Rate (MGD)	268	263	257	256		125	119	92	93
PO_4 (μM)	5.5	5.3	3.8	3.5		23.4	34.6	26.5	24.2
NO_2 (μM)	3.9	6.1	15.1	6.2		196	238	152	170
NO_3 (μM)	5.1	4.2	10.5	6.5		883	852	784	850
NH_4 (μM)	2690	3460	2670	1260		1890	1460	1800	2990
DIN	2699	3470	2695	1273		2969	2550	2736	4010
DIN Loading (g/day)	3.8 x10^7	4.8 x10^7	3.7 x10^7	1.7 x10^7		1.9 x10^7	1.6 x10^7	1.3 x10^7	2.0 x10^7
N:P	490	652	1540	852		127	74	103	94
DOC (μM)	1107	1174	1379	1918		1186	1129	1497	2241
DIC (μM)	4900		4361	2750		5076	6398	4404	2909
$\delta^{15}N_{NO2+NO3}$ (‰)	-9.6	-2.3				9.1	7.5		
$\delta^{18}O_{NO2+NO3}$ (‰)	-15.2	-15.6				-5.8	-3.5		
$\delta^{15}N_{NH4}$ (‰)	7.5	5.1	9.6	12.4		9.1	8.9	8.6	9.1
e_{nit}	-17.1	-7.4				0	-1.9		

Table 3. Spearman rank correlations between dissolved and particulate variables.

Color scale indicates the correlation coefficient, where red indicates positive correlation, blue negative, white is 0 (no correlation). Stars indicate significance where * is $p < 0.05$, ** where $p < 0.01$, and *** where $p < 0.001$. Parameters were ordered using hierarchical clustering.

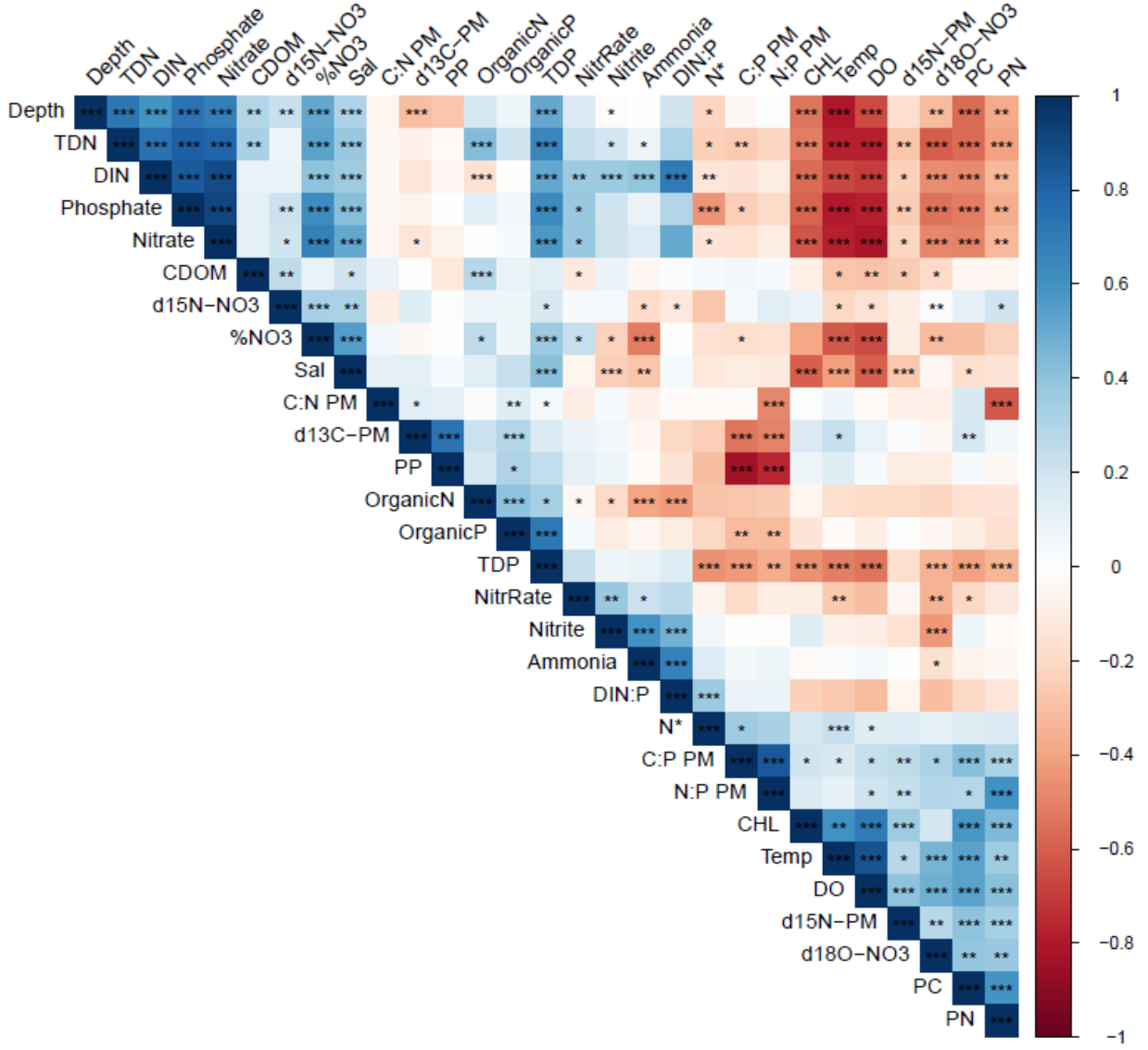

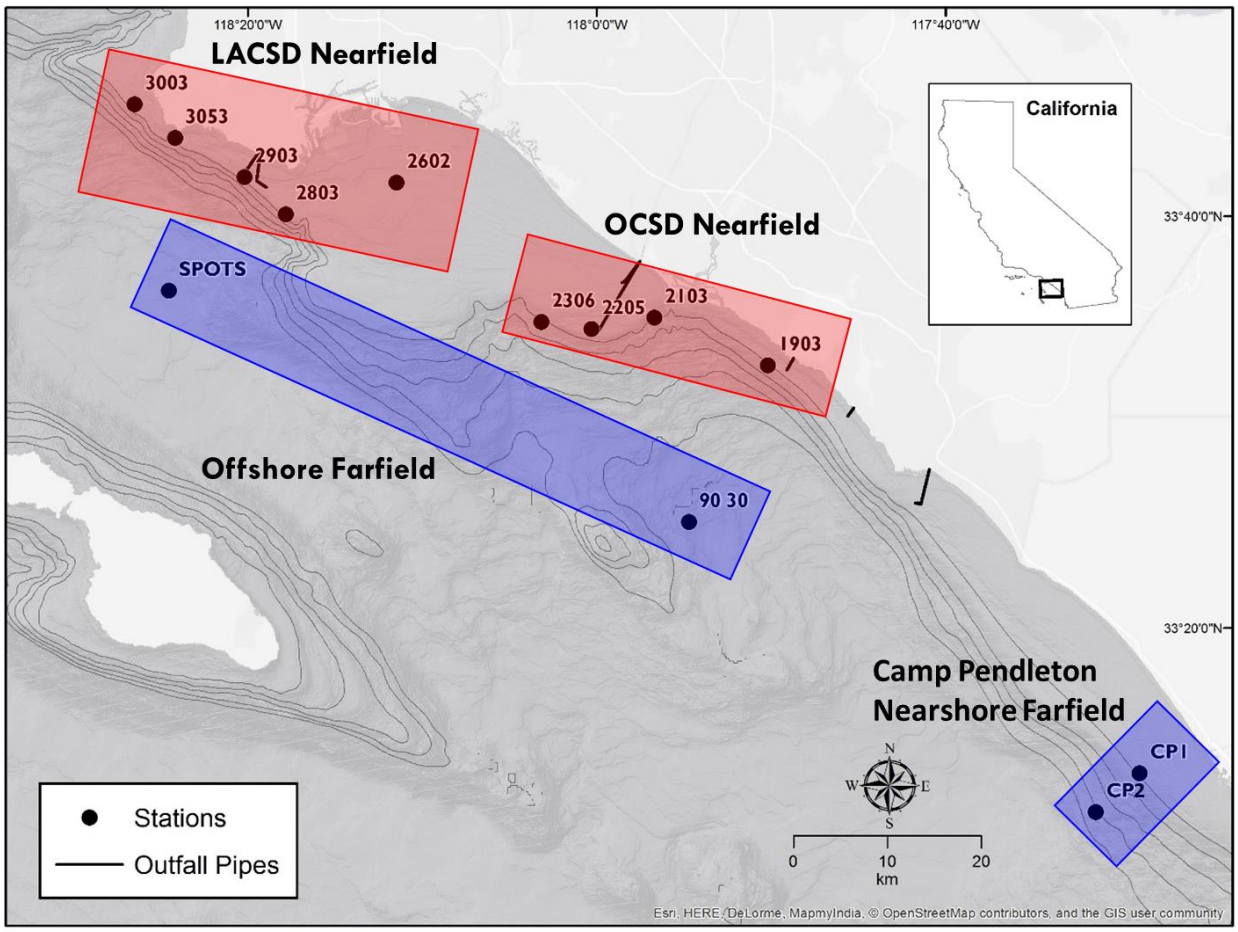

Figure 1. Station Locations. The nearfield sub-regions are shown in red and include LACSD and OCSD grid stations. The farfield (reference) sub-regions spatially distant from the outfalls are shown in blue and include 2 offshore stations (SPOTS and CalCOFI 90.30) and 2 nearshore stations located by Camp Pendleton, in northern San Diego County (CP1 and CP2). CTD casts were collected at additional stations within the regulatory monitoring grids around both LACSD's and OCSD's ocean outfalls to determine the location of the plume at the time of sampling to select the second plume station.

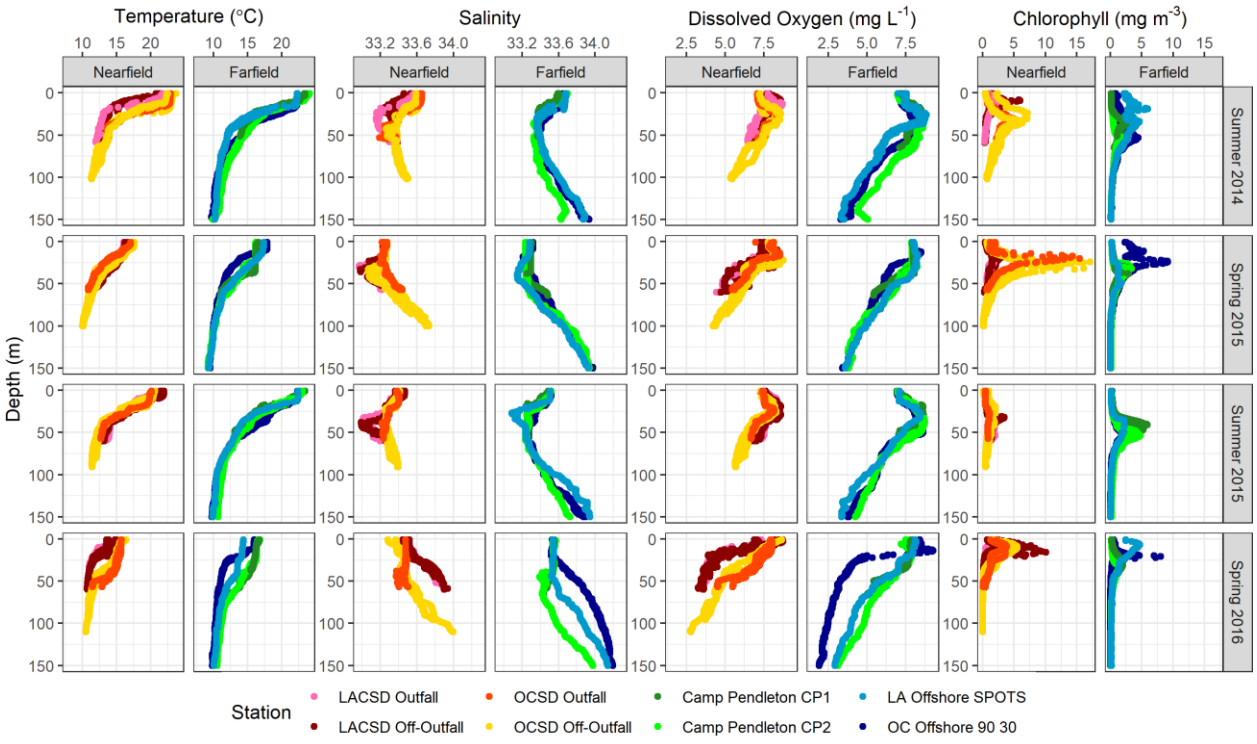

Figure 2. Spatial and temporal patterns in temperature, salinity, dissolved oxygen, and chlorophyll during each sampling event. Figure is faceted by nearfield stations and farfield stations for each parameter and by season. Each subregion was sampled in a different week in a single month, introducing some temporal variability into the dataset within a season. Plume is generally located between 20 and 60 m depth in the nearfield sites (Figure SI.1).

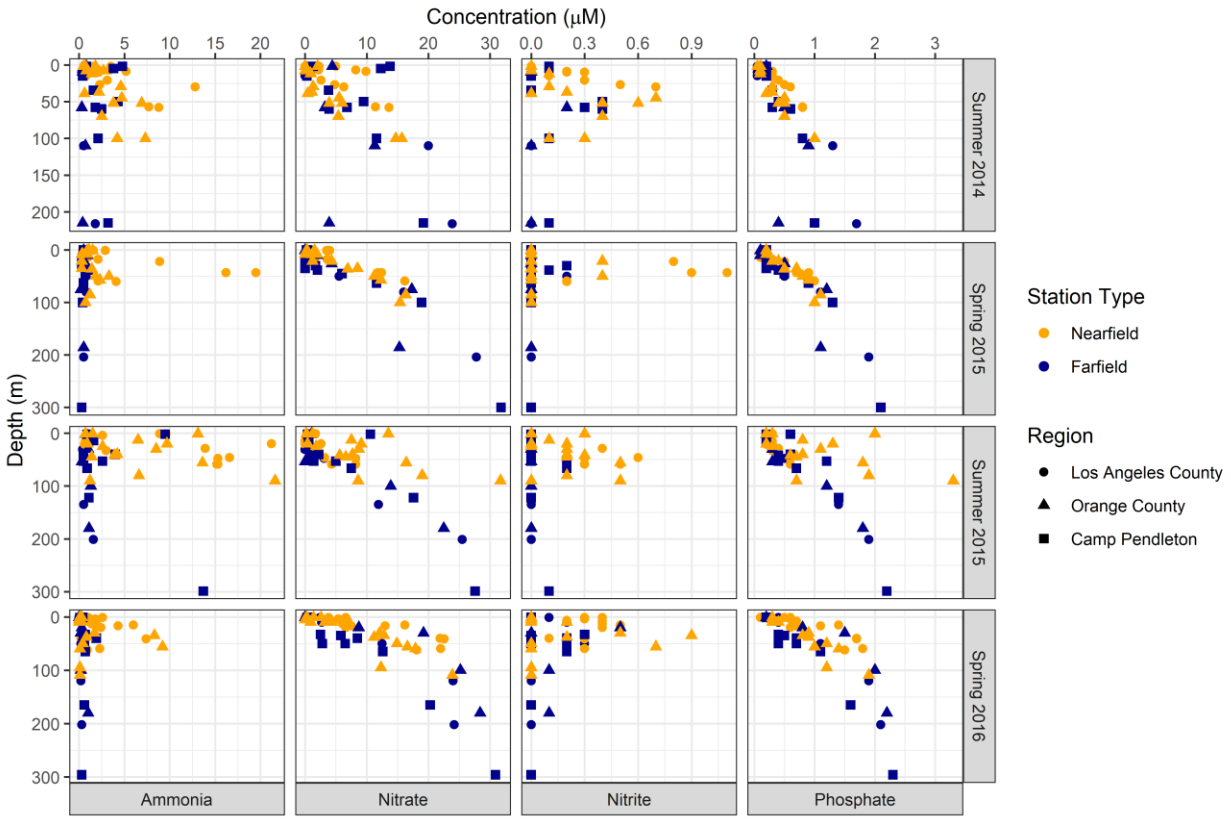

Figure 3. Depth profiles of dissolved inorganic phosphate, ammonia, nitrite, and nitrate. Plume is generally located between 20 and 60 m depth in the nearfield sites (Figure SI.1).

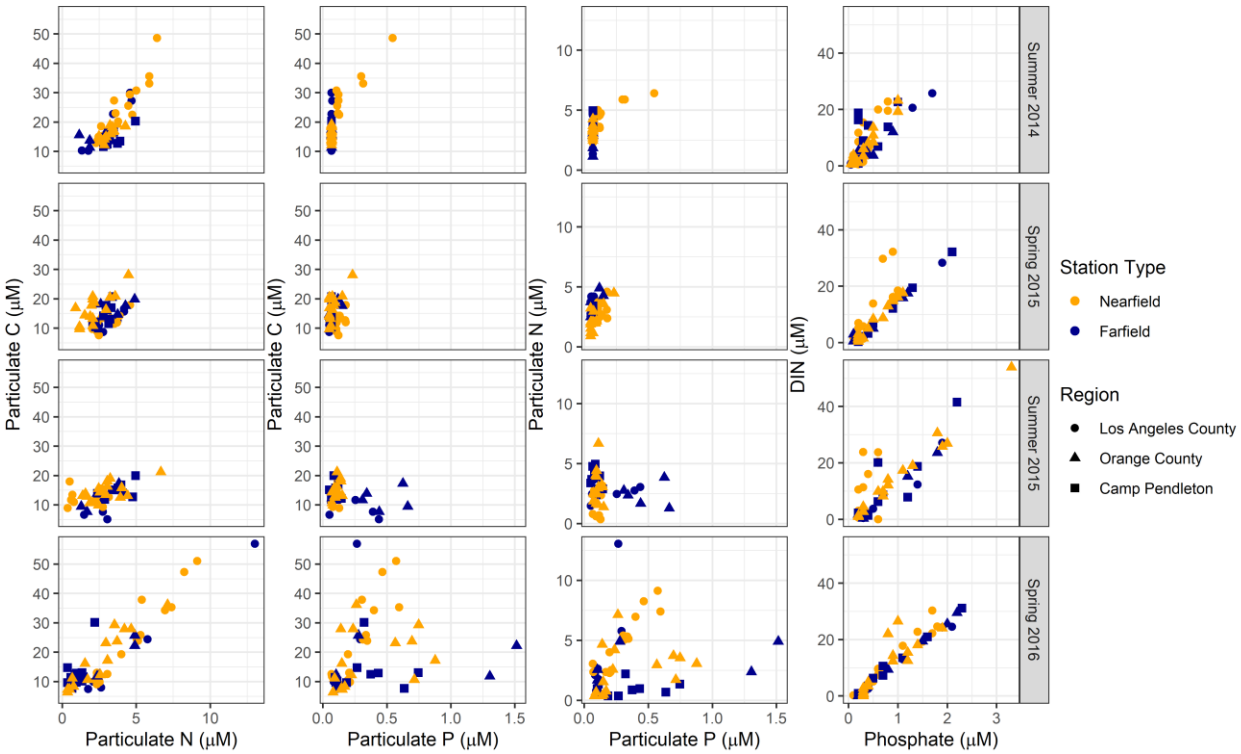

Figure 4. Property-property plots for dissolved and particulate nutrients. Particulate carbon as a function of particulate nitrogen and particulate phosphorus, particulate nitrogen as a function of particulate phosphorus, and dissolved inorganic nitrogen (DIN) as a function of dissolved phosphate.

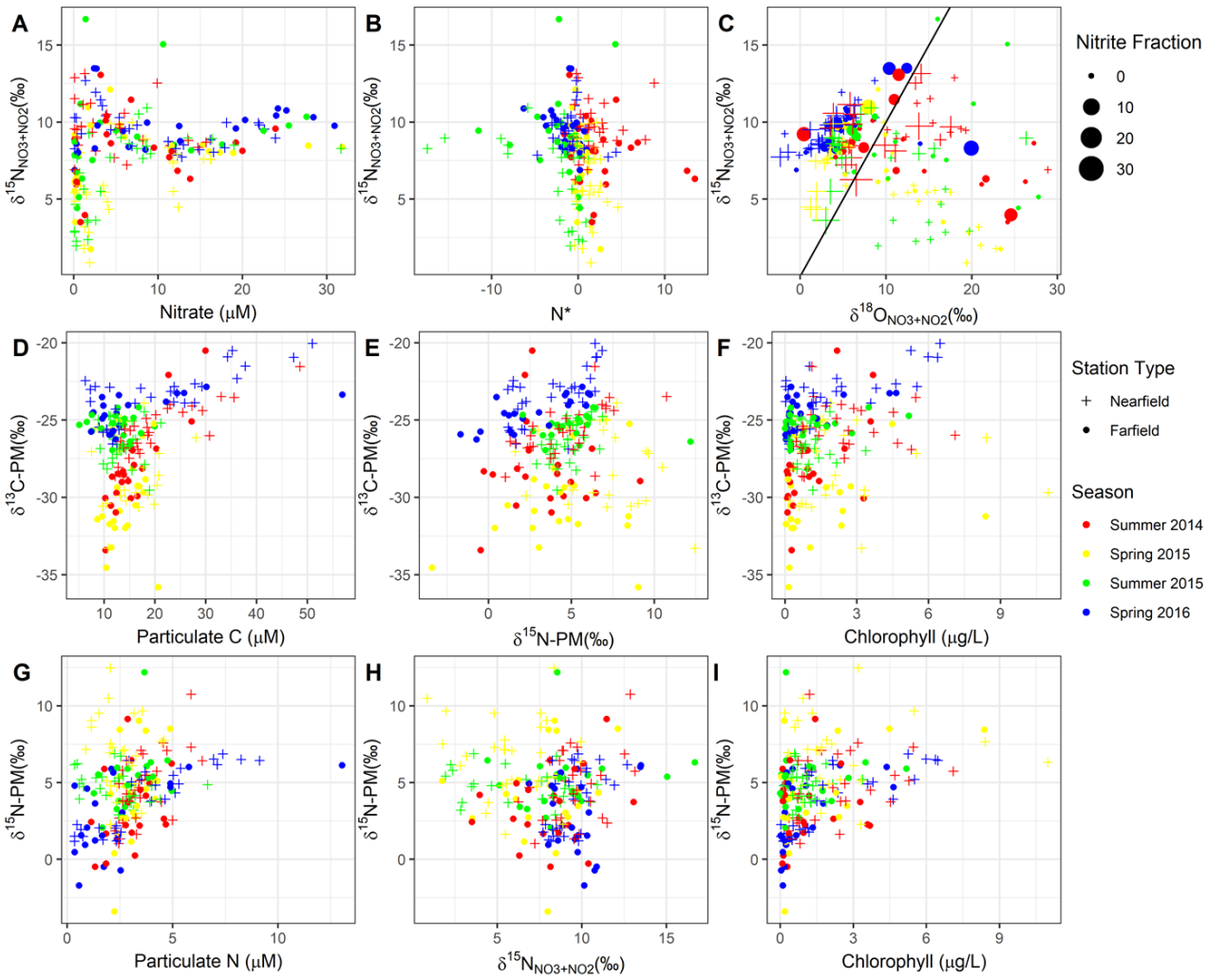

Figure 5. Property-property plots of $\delta^{15}N_{NO3}$ and nitrate concentration (A), $\delta^{15}N_{NO2+NO3}$ and N* (B), and $\delta^{15}N_{NO2+NO3}$ and $\delta^{18}O_{NO2+NO3}$, where the black line represents 1:1 (C), $\delta^{13}C_{PM}$ and particulate carbon concentration (D), $\delta^{13}C_{PM}$ and $\delta^{15}N_{PM}$ (E), $\delta^{13}C_{PM}$ and chlorophyll *a* (F), $\delta^{15}N_{PM}$ and particulate nitrogen concentration (G), $\delta^{15}N_{PM}$ and $\delta^{15}N_{NO2+NO3}$ (H), $\delta^{15}N_{PM}$ and chlorophyll *a* (I). Colors represent the seasons; shapes represent the station types. The size of the points only applies to the nitrite fraction in panel (C) where increased fraction nitrite in the nitrite+nitrate may underestimate $\delta^{18}O_{NO2+NO3}$. Supplemental Figure SI.12 shows how this underestimation may effect results.

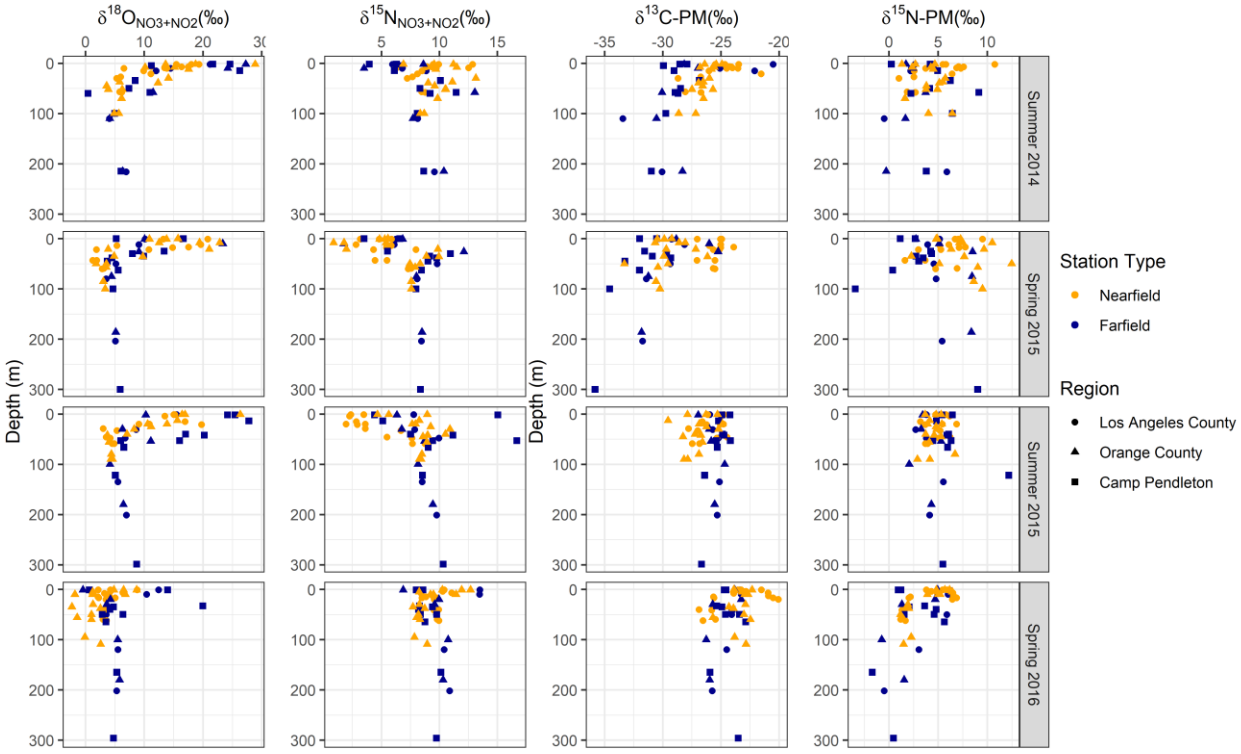

Figure 6. Depth profiles of dissolved $\delta^{15}N_{NO3}$ and $\delta^{18}O_{NO3}$, and particulate $\delta^{13}C_{PM}$ and $\delta^{15}N_{PM}$. Plume is generally located between 20 and 60 m depth in the nearfield sites (Figure SI.1).

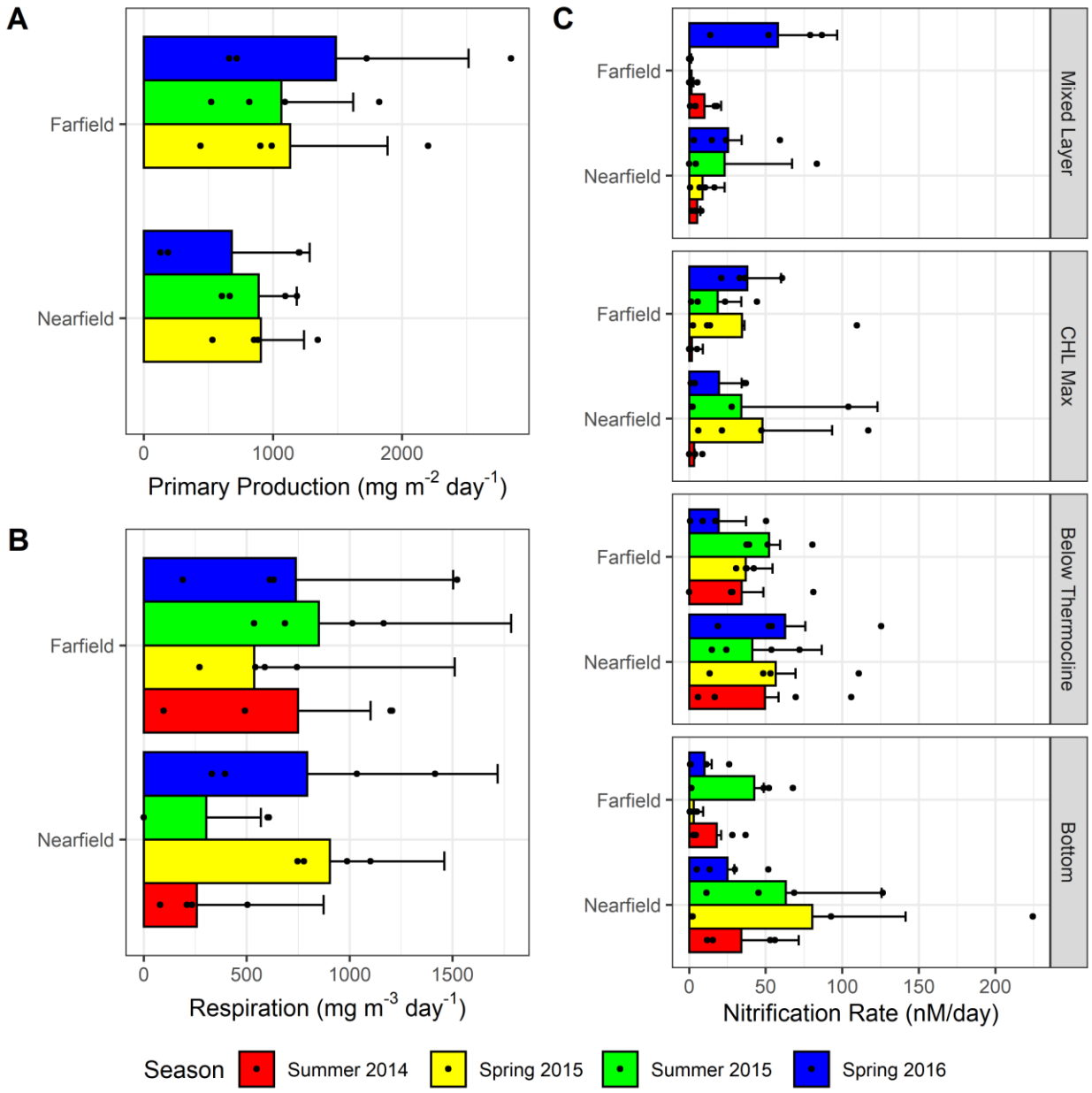

Figure 7. Depth integrated primary production rates (A), average subsurface respiration rates (B), and nitrification rates faceted by depth layer (C) by station type. Black points represent individual data points. There was no data collected of primary production in Summer 2014. Error bars for indicate the standard deviation.

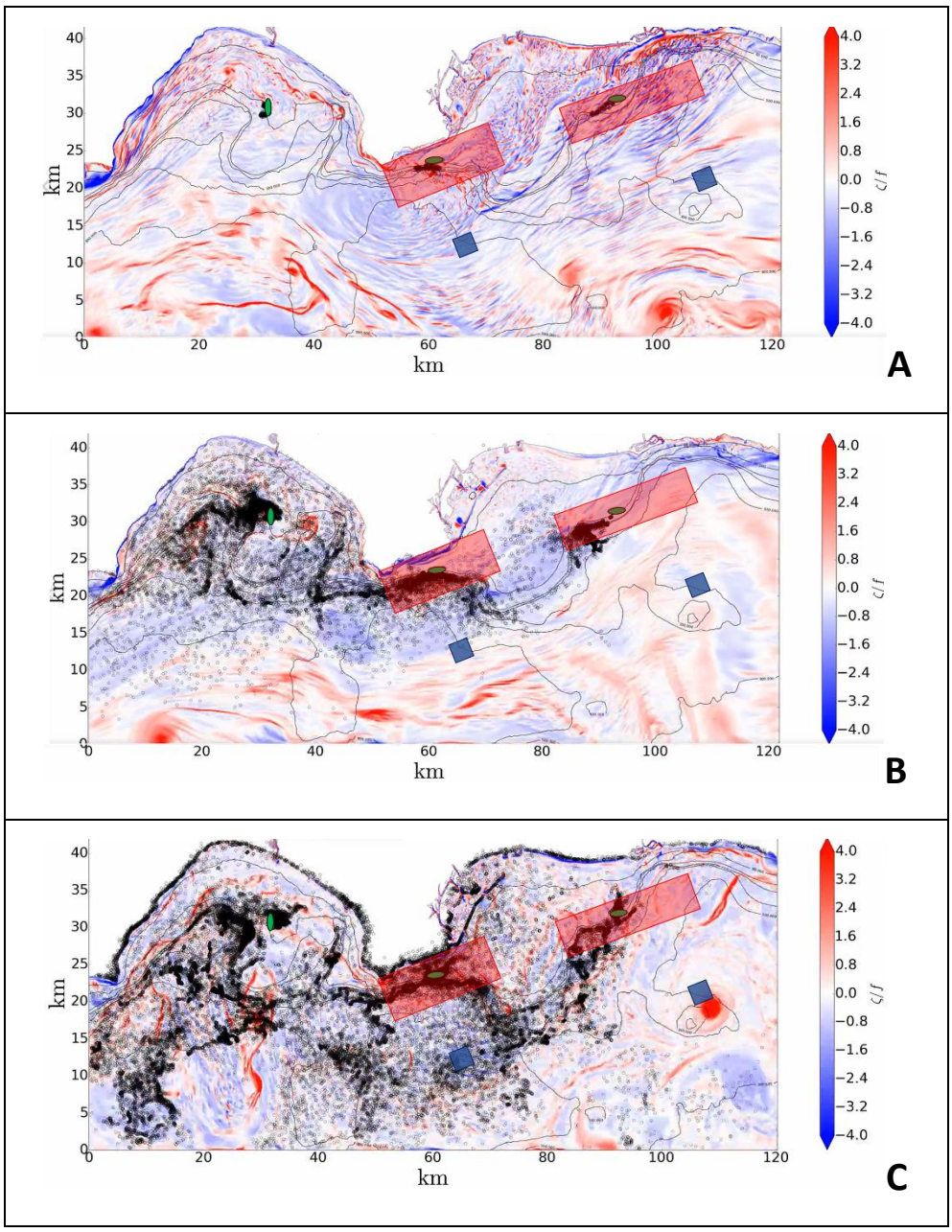

Figure 8. Downscaled Regional Ocean Model (350 m scale) run in particle tracking mode demonstrating the fate of wastewater effluent released from ocean outfalls. Color bar represents the Coriolis-normalized vorticity (a measure of ocean stirring). Black circles represent particles released from outfalls (green ovals). Red boxes are nearfield areas and blue boxes represent farfield, offshore areas. Panel A shows particle distribution 9 hours from the start of the simulation on January 1 at 01:00). Two weeks into the simulation, particles are nearly completely mixed in the nearshore areas (Panel B). Panel C shows the end of the simulation, two months, particles released from the outfalls have been mixed to the offshore regions (Dauhajre et al. 2019).

SUPPLEMENTAL MATERIALS

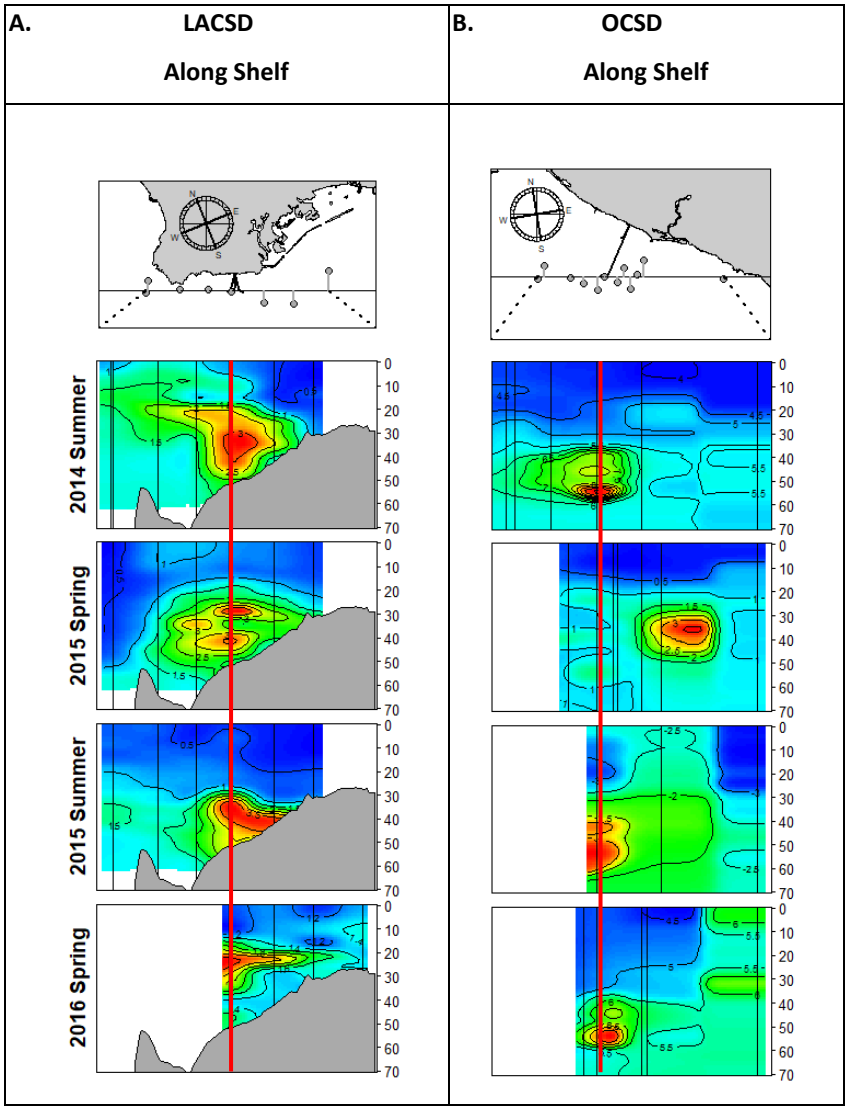

Figure SI.1. Spatial extent of the effluent plumes during each of the sampling events as measured by CDOM (mg m^{-3}). Note colored scale on each graphic is different, scaling was free on each figure to demonstrate the extent of the plume. Scales are plotted from the minimum reported value to the maximum for each site to identify the plume locations over each outfall. Each CTD cast location is represented by a black vertical line, multiple casts were taken to determine the direction of the plume during sampling events and not all stations correspond to sampling locations on Figure 1. The station sampled over each outfall is highlighted in red.

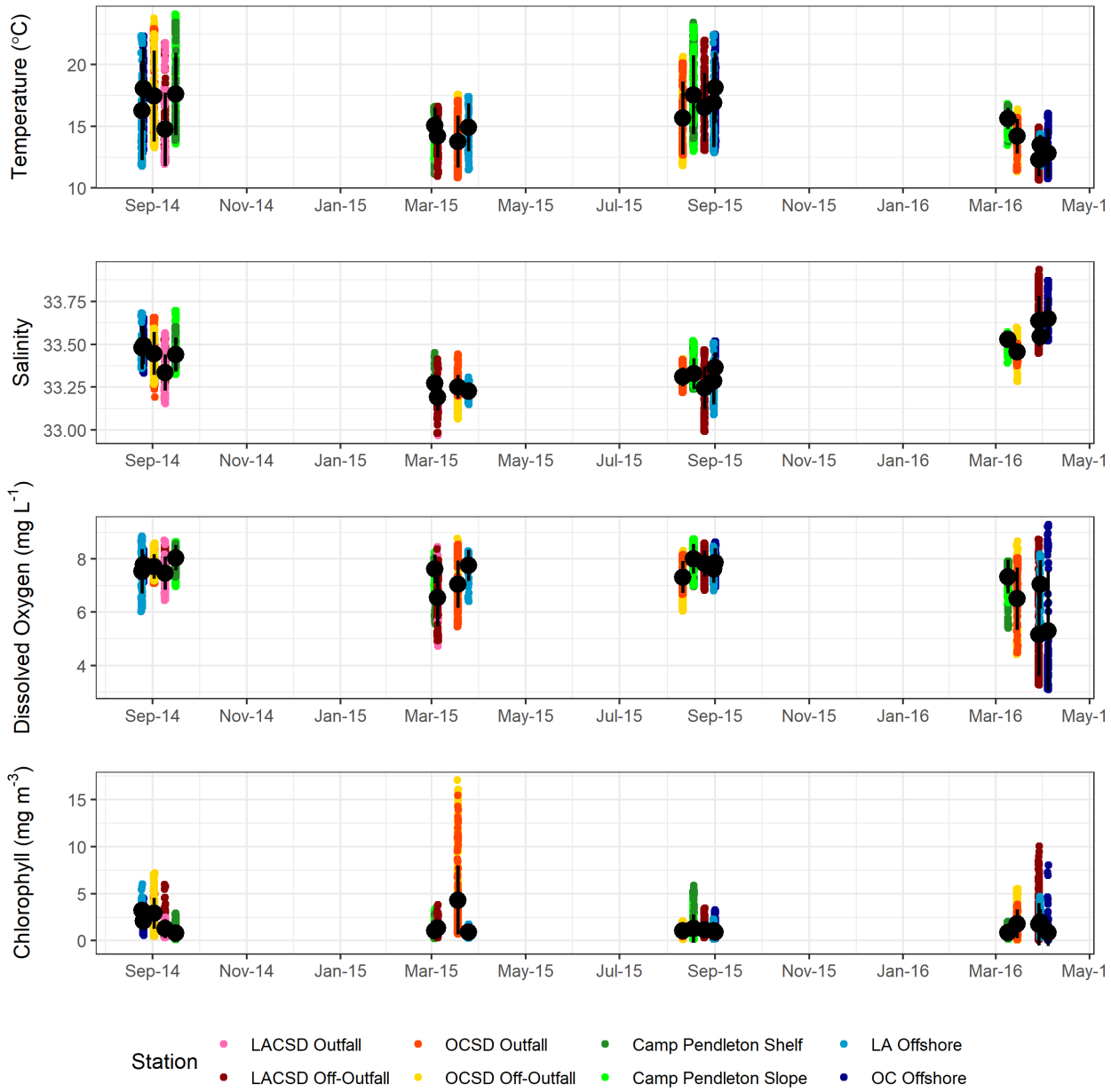

Figure SI.2. Timing of sampling and ranges of data for upper 60 m at each site. Black dot represents the mean and bar the standard deviation of all values in upper 60 m.

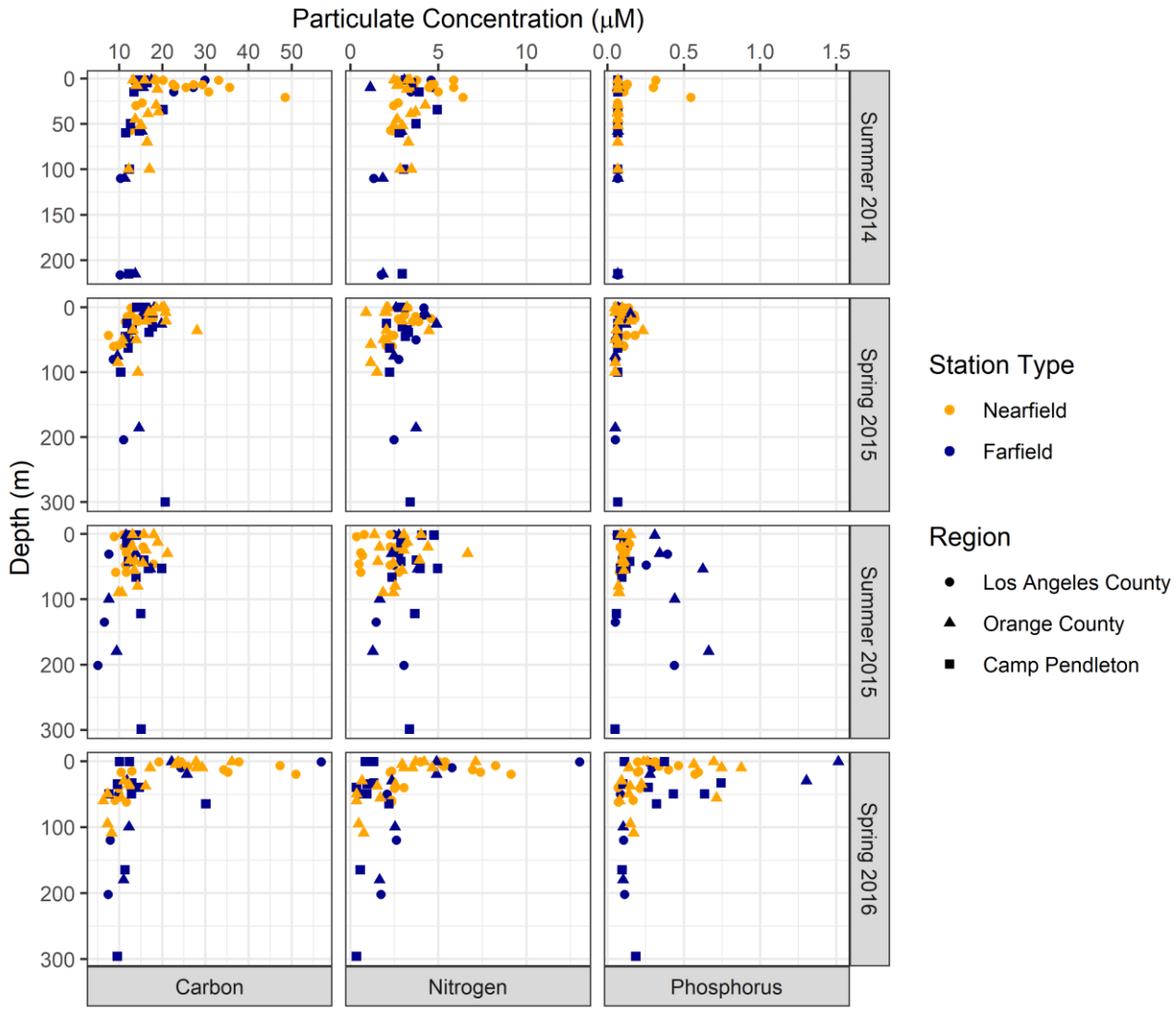

Figure SI.3. Depth profiles of particulate carbon, nitrogen and phosphorus. Plume is generally located between 20 and 60 m depth in the nearfield sites.

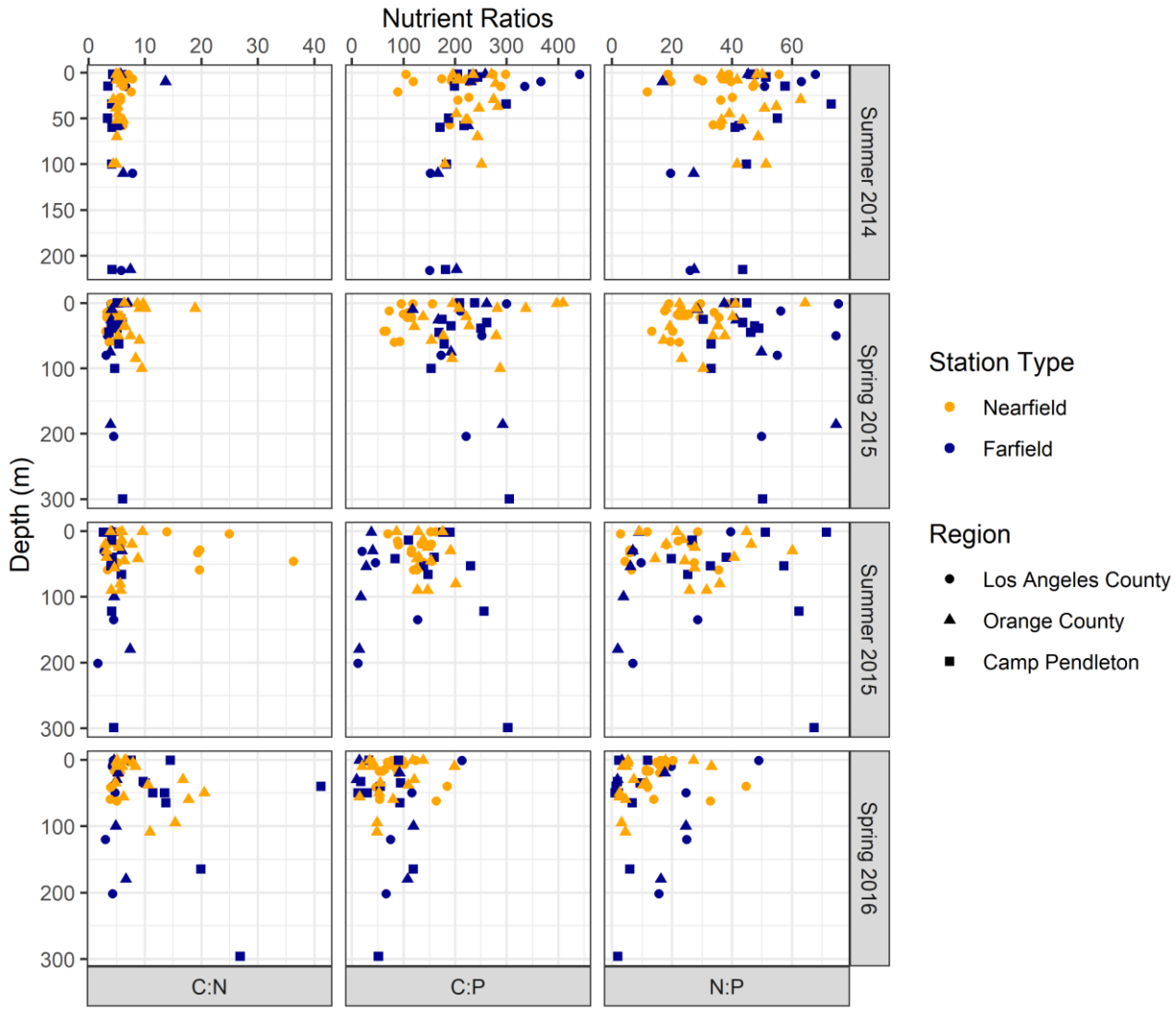

Figure SI.4. Depth profiles of particulate C:N, C:P, and N:P. Plume is generally located between 20 and 60 m depth in the nearfield sites.

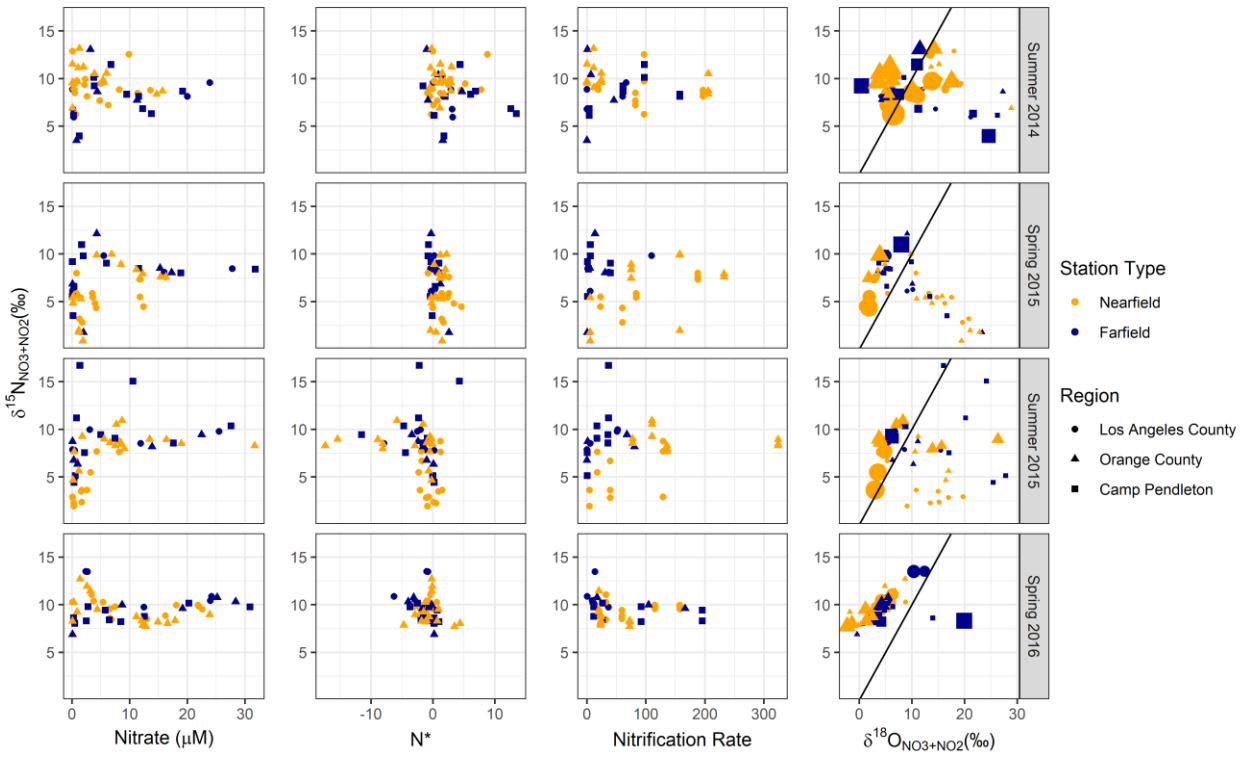

Figure SI.5. The $\delta^{15}N_{NO2+NO3}$ as a function of nitrate concentration, N*, nitrification rate, and $\delta^{18}O_{NO2+NO3}$. The black line in the final column represents a 1:1 relationship between the relative enrichment of the two isotopes. The size of the points represents the fraction of nitrite in the nitrite+nitrate measured in each sample; larger points have higher fraction of nitrite.

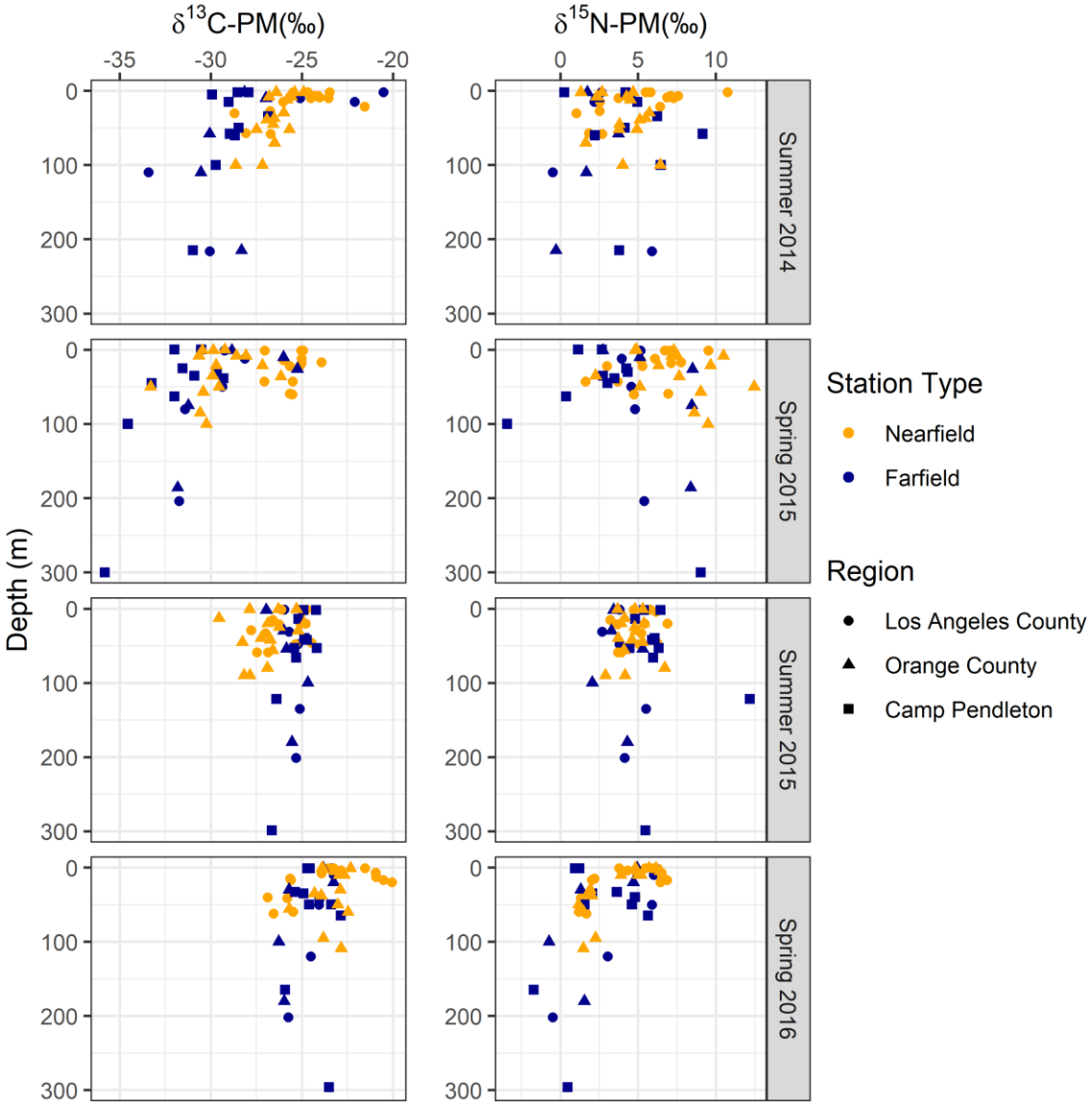

Figure SI.6. Depth profiles of the stable isotopic composition of particulate carbon ($\delta^{13}C_{PM}$) and nitrogen ($\delta^{15}N_{PM}$). Plume is generally located between 20 and 60 m depth in the nearfield sites.

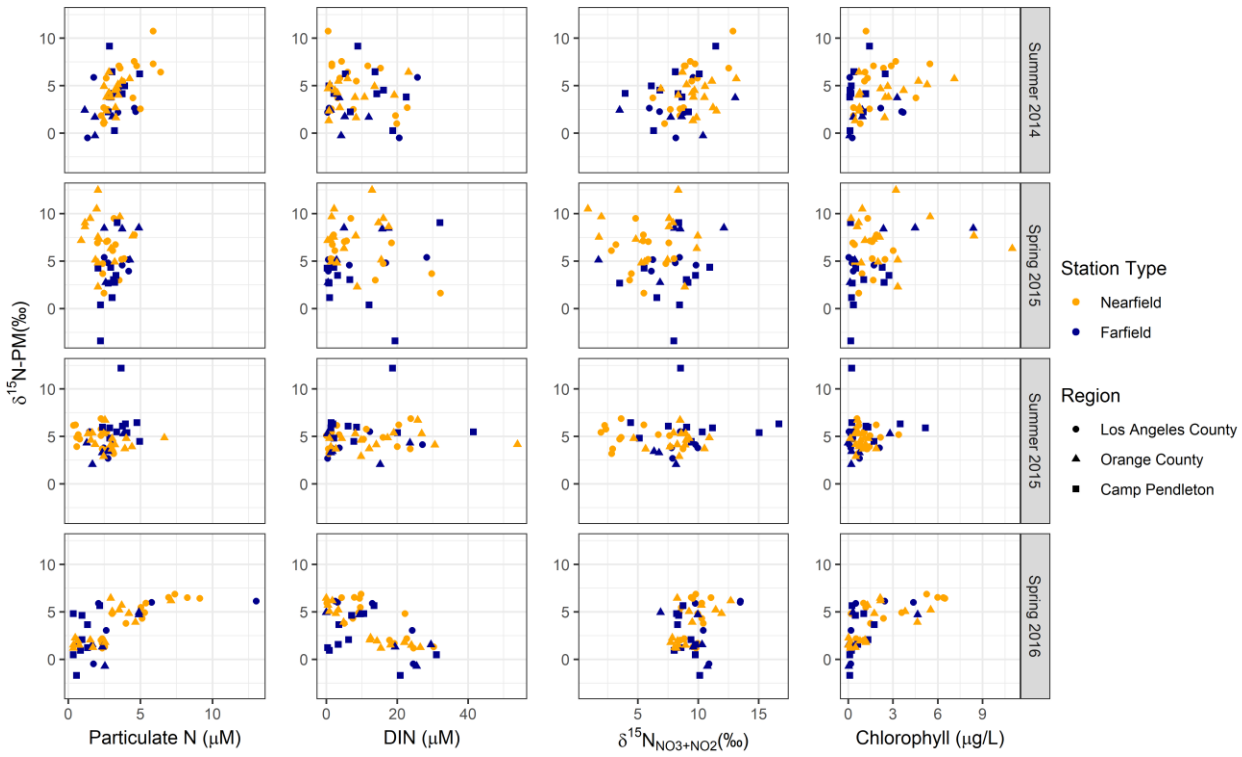

Figure SI.7. The $\delta^{15}N_{PM}$ as a function of particulate nitrogen concentration, dissolved inorganic nitrogen (DIN), $\delta^{15}N_{NO2+NO3}$, and chlorophyll *a* concentration.

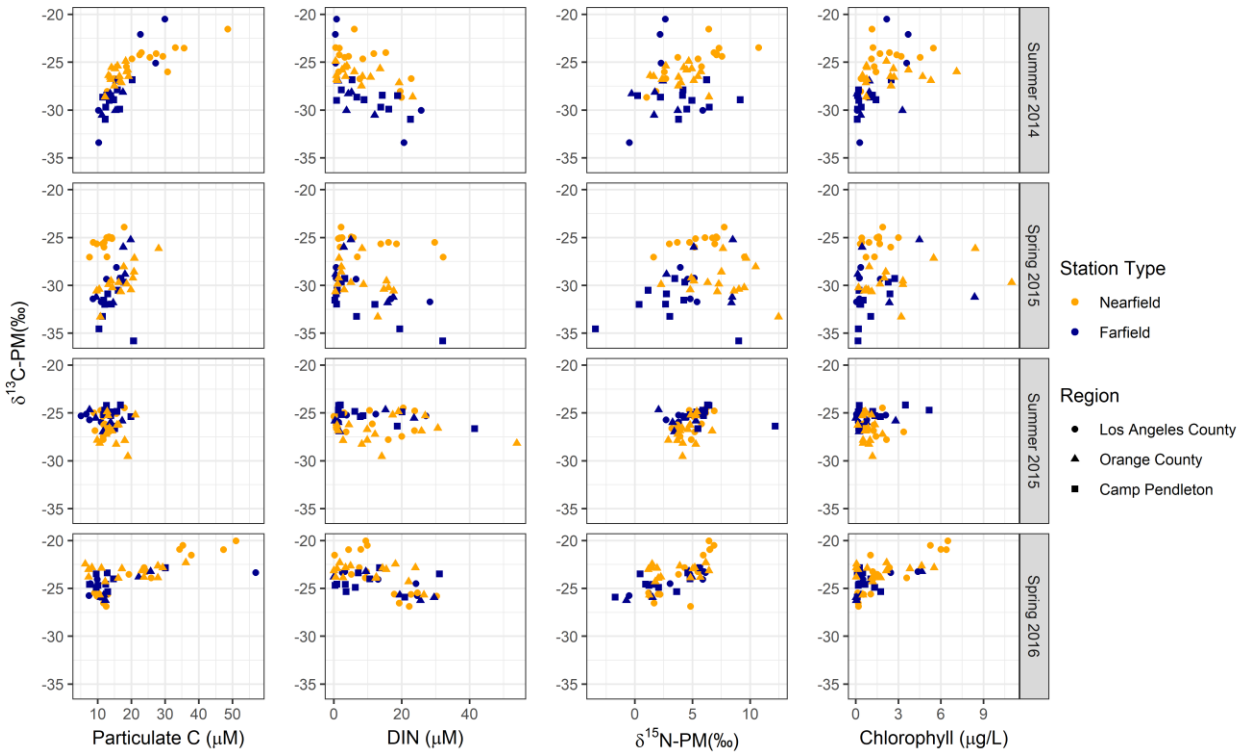

Figure SI.8. $\delta^{13}C_{PM}$ as a function of particulate carbon, DIN, $\delta^{15}N_{PM}$, and chlorophyll *a* concentration.

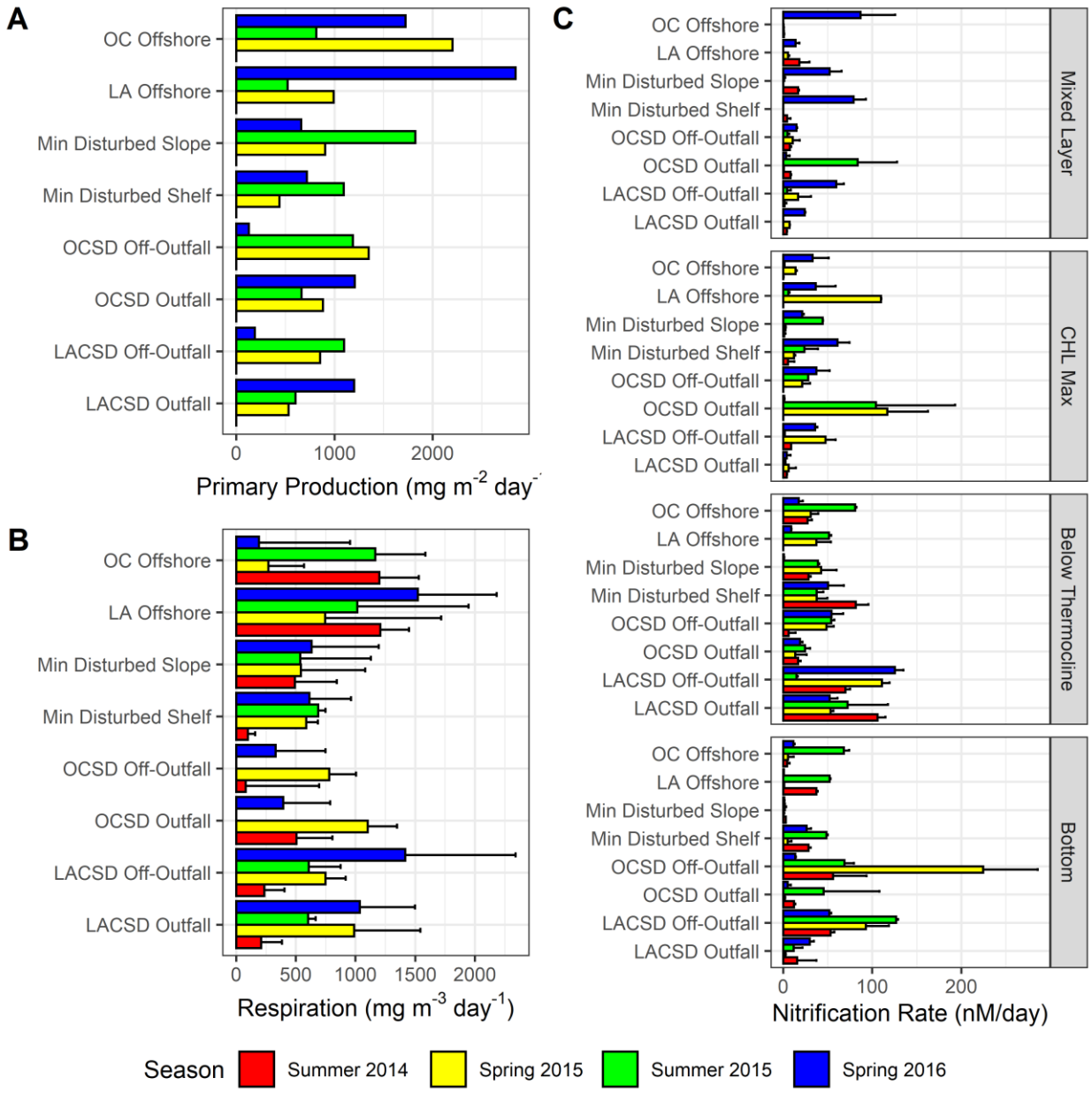

Figure SI.9. Depth integrated primary production rates (A), average subsurface respiration rates (B), and nitrification rates faceted by depth layer (C) by station. There was no data collected of primary production in Summer 2014. Error bars for indicate the standard deviation.

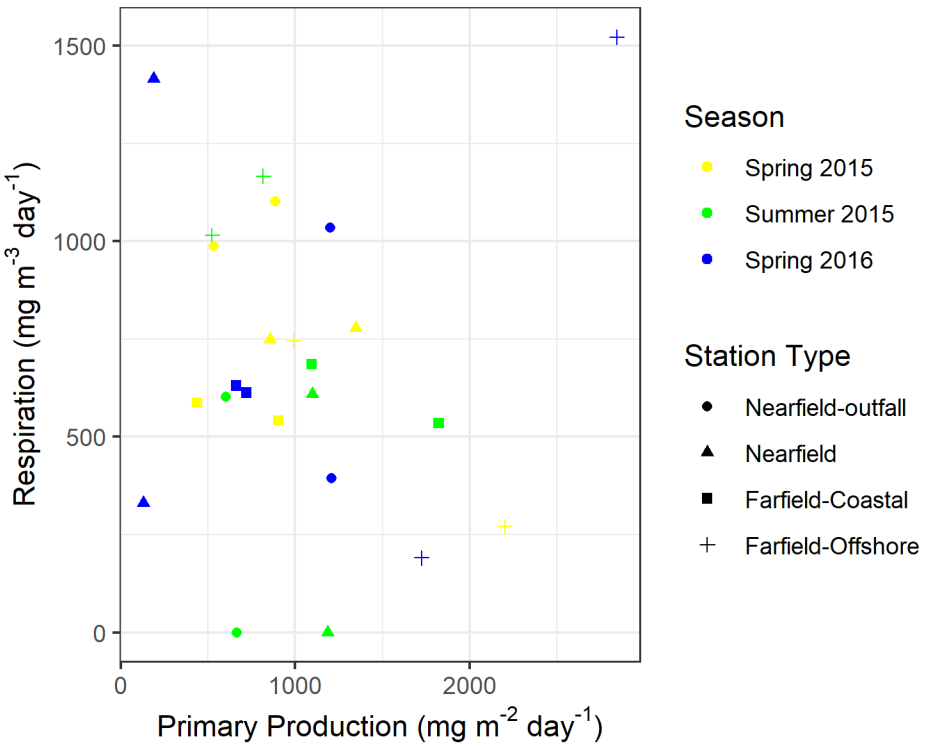

Figure SI.10 Relationship between depth integrated primary production and average subsurface respiration for the three-time periods when both parameters were measured.

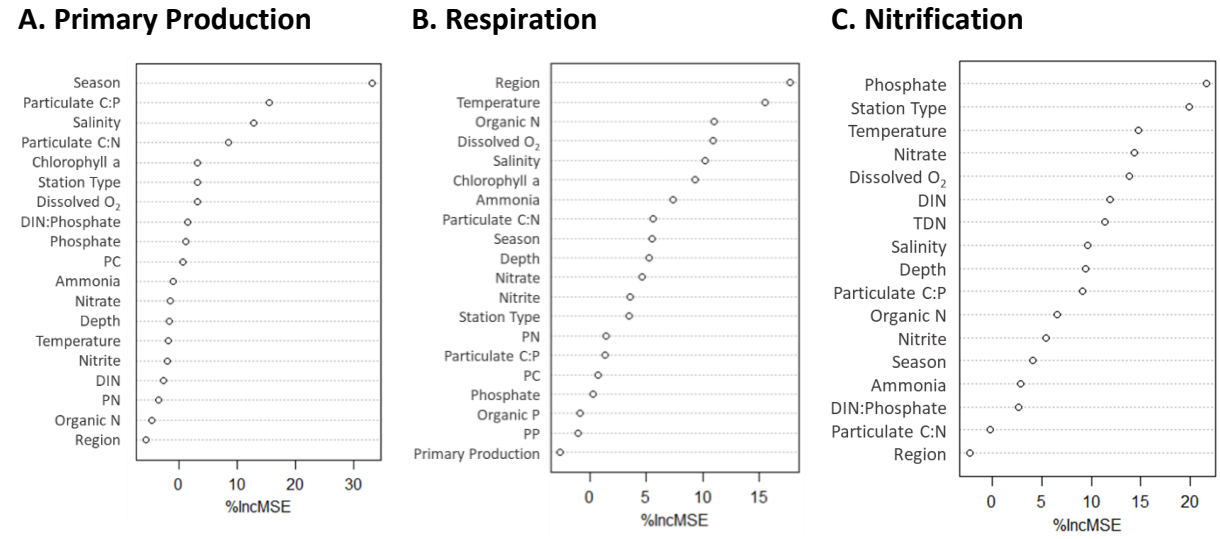

Figure SI.11. Variable importance from random forest regression models predicting primary production (A), respiration (B), and Nitrification (C). Predictor variables were plotted with their increase in percent mean squared error (%IncMSE) when the variable is randomly permuted in the model, higher values indicate variables were more important to the regression. The overall percent variance explained using the random forest models was 30% for primary production, 18% for respiration, and 20% for nitrification.

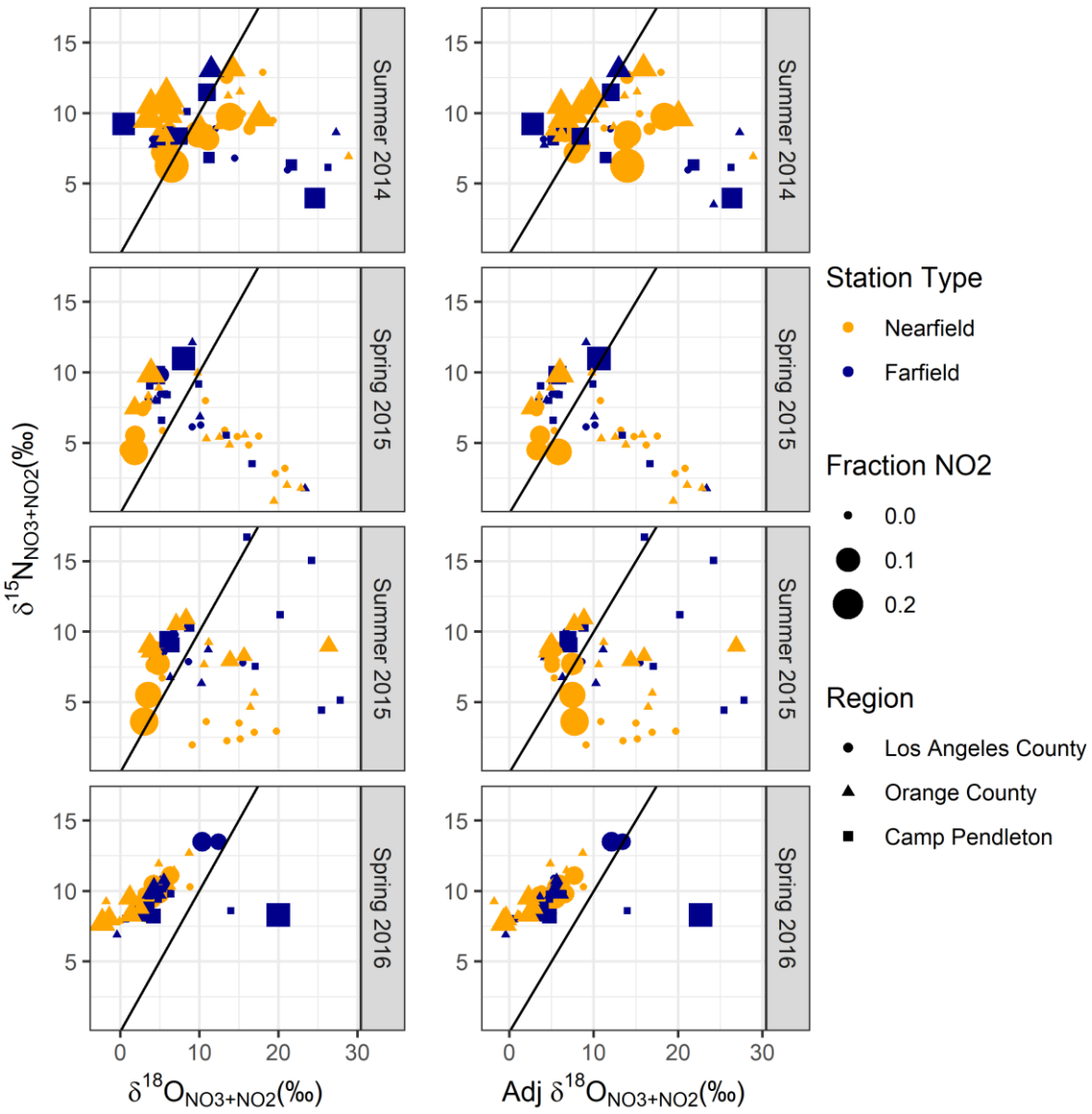

Figure SI.12. Estimation of the impact of high nitrite on the $\delta^{18}O_{NO2+NO3}$. For samples with high nitrite concentrations, the denitrifier method employed in this study for oxygen isotope analysis of dissolved nitrate + nitrite is expected to underestimate the oxygen isotopic composition of nitrite by 25-30‰. We calculated the fraction of nitrite in each sample and estimated the impact of a 25‰ underestimation of the $\delta^{18}O_{NO2}$ on the final $\delta^{18}O_{NO2+NO3}$ (Adj $\delta^{18}O_{NO2+NO3}$ right panel). Values were increased an average of 2.7 ‰ with a maximum increase of 13.8 ‰. Samples with the highest fraction of nitrite (indicated by the size of the point), had the greatest increase.